Supporting Information for

Measurement of Energy Landscape Roughness of Folded and Unfolded Proteins

Lilia Milanesi[a,b], Jonathan P. Waltho[a,c], Christopher A. Hunter[b], Daniel J. Shaw[d], Godfrey S. Beddard[d], Gavin D. Reid[d], Sagarika Dev[e], and Martin Volk[e,1]

[a]Department of Molecular Biology and Biotechnology, University of Sheffield, Sheffield S10 2TN, UK;
[b]Department of Chemistry, University of Sheffield, Sheffield S10 2TN, UK;
[c]Manchester Institute of Biotechnology, 131 Princess St., Manchester. M1 7DN, UK;
[d]School of Chemistry, University of Leeds, Leeds LS2 9JT, UK;
[e]Department of Chemistry, University of Liverpool, Liverpool L69 3BX, UK.

[1]To whom correspondence should be addressed: m.volk@liv.ac.uk

Appendix I: Materials and Methods

Sample Preparation. Disulfide cross-linked N-PGK in 50 mM sodium phosphate buffer, pD 6.6-7, 100 mM NaCl was prepared as described in reference (1) and urea added as indicated. Figure S1 shows that the addition of 2 M urea has no effect on the secondary structural content of the open form of N-PGK, and only a small effect on the total secondary structural content of the cross-linked form.

Measurements on the ps-time scale. A fs-oscillator and regenerative amplifier system (Spectra Physics, Tsunami and Spitfire) was used to produce laser pulses at 800 nm of 50 fs pulse length and 800 μJ energy at a repetition of 1 kHz, which were used to seed two optical parametric amplifiers (OPA, Spectra Physics OPA 800C). The output of one OPA was doubled externally to 275 nm in a 100 μm BBO crystal, yielding pulses of 100 fs length and 1.5 μJ energy, which were focused to a spot of 0.5 mm diameter on the sample and used as pump pulses. Probe pulses of 100 fs pulse length at 560 nm were obtained from the second OPA and delayed with respect to the pump pulses via an optical delay line. The probe polarization was adjusted to be at magic angle to the pump polarization. Time zero and cross correlation were determined using Rhodamine 6G in methanol. Transient absorption changes were measured by reducing the excitation rate to 500 Hz with a mechanical shutter, thus allowing simultaneous detection of the absorption with and without pumping.

A quartz suprasil cell (pathlength 1 mm) with 10-20 μM cross-linked N-PGK in 50 mM deuterated sodium phosphate buffer, pD 6.6, 100 mM NaCl, was used. The cell was slowly rotated to avoid sample degradation. The results shown here are the average of many scans over different delay times. No signal degradation was observed during these scans. Similarly, UV/vis absorbance spectra taken before, during and after the measurements showed no changes, confirming sample stability.

Measurements on the ns- to ms-time scale. Pulses from the fourth harmonic output of a Nd:YAG laser (Quantel Brilliant) at 266 nm with a pulse length of 5 ns were used to photolyse the sample at a repetition rate of 10 Hz. The pulse energy was adjusted to 0.3 mJ, which was focused to a spot size of approx. 1 mm on the sample.

Transient absorbance changes were probed with cw light, focused to a spot size of less than 0.5 mm on the sample, and detected with a fast Si-detector (Thorlabs DET210, rise time 1 ns) and an oscilloscope (Tektronix TDS3032, bandwidth set to 20 MHz, resulting in an overall signal rise time of approx. 20 ns). For preliminary experiments, cw light from a xenon lamp (Applied Photophysics Ltd. 4960) was used for probing, from which particular wavelength regions were selected using interference band pass filters (band width 40 nm). These experiments showed that photolysis of the disulfide cross-link resulted in a transient species with a maximum absorbance around 500 nm, confirming the formation of thiyl radicals. For the dynamic measurements with better signal-to-noise shown in Fig. 3B-D, 6 mW cw light from an argon-ion laser (Ion Laser Technology 5450AWC) at 488 nm was used for probing.

A solution of approx. 600 μM cross-linked N-PGK in 50 mM sodium phosphate buffer, pH 7.0, 100 mM NaCl, 2 M or 8 M deuterated urea, was continuously flowed through a cell (pathlength 0.25 mm) with a peristaltic pump. The results shown here are the average of more than 5,000 single measurements. No signal degradation was observed during this time.

Data Treatment. The data shown in Fig. 3 are raw results obtained from the measurements, after averaging over repeated scans. Before calculating the instantaneous rate constant, $k_{inst}=-(dc/dt)/c$, shown in Fig. 4, the data from Fig. 3 were smoothed by combining all data points within a progressively increasing time window (with a width of +/-10% of the centre time) into one averaged point. Fitting of the instantaneous rate constant to a power law was performed using linear fits on a log-log scale, as shown in Fig. 4.

Appendix II: CD Spectra and Unfolding Curves of Open and Cross-linked N-PGK

CD spectra were recorded in absence and presence of varying concentrations of urea on samples with a protein concentration of 20 µM in 50 mM sodium phosphate buffer, pH 7.0, 100 mM NaCl. The open form of N-PGK was obtained by addition of 1 mM DTT. Samples were allowed to denature for 4 hours at 25°C prior to addition of DTT and recording of spectra. All CD spectra were recorded between 200 and 280 nm in a cell with a pathlength of 1 mm, using a scanning speed of 50 nm/min and a response time of 8 s. The spectra were averaged over 2 scans at 0.1 nm resolution and a bandwidth of 2 nm. The observed ellipticity, θ (millidegree) was converted to molar ellipticity $[\theta]$.

Figure S1a shows CD spectra of open and cross-linked N-PGK. The spectra show that in the absence of denaturant, cross-linked and open N-PGK have similar secondary structural content, although the difference in the CD-spectra indicates different overall structure. Fluorescence and NMR spectroscopy confirm that the structure of cross-linked N-PGK is less ordered and more molten-globule like in the absence of denaturant (1). Upon addition of 2 M urea, cross-linked N-PGK shows decreased secondary structural content, whereas open N-PGK is still fully folded. Addition of 8 M urea, on the other hand, yields a similar loss of structure in cross-linked and open N-PGK.

Figure S1b shows the unfolding curves of open and cross-linked N-PGK, determined from the CD-signal $[\theta]$ at 222 nm, normalized to the signal at 0 M urea, against urea activity, D = [urea] × $C_{0.5}/(C_{0.5}$+[urea]), where [urea] is the molar concentration of urea and $C_{0.5}$ = 25.3 M (2). The data were fitted to a two-state model, assuming constant baselines, yielding the following results (referring to the plot of $[\theta]/[\theta]_0$ *vs*. urea activity):

Open N-PGK

ΔG_0 = (-7.2 ± 0.5) kcal/mol m = (-2.9 ± 0.2) M^{-1}

Cross-linked N-PGK

ΔG_0 = (-2.2 ± 0.1) kcal/mol m = (-1.1 ± 0.05) M^{-1}

The value of ΔG_0 for open N-PGK is in reasonable agreement with the value of (-8.3 ± 0.4) kcal/mol determined previously for the same protein from GuHCl-induced unfolding, detected by tryptophan fluorescence (1). Due to the absence of clear baselines, the values for cross-linked N-PGK have to be regarded as crude estimates only.

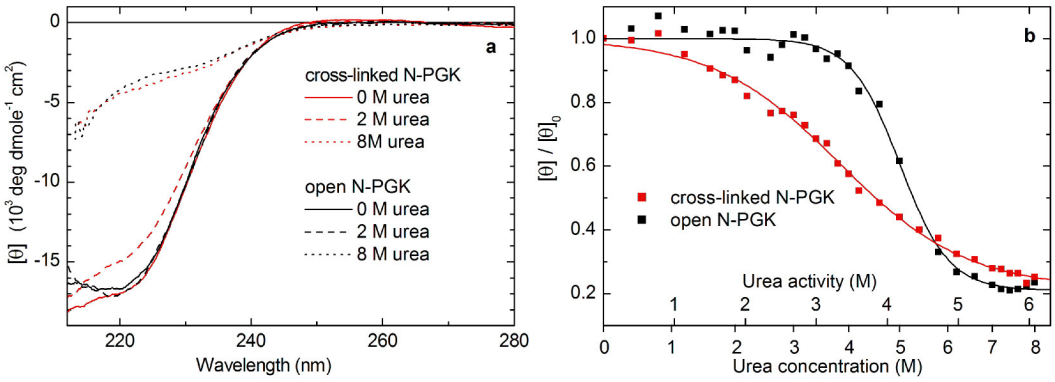

Figure S1. Denaturant-induced unfolding of open and cross-linked N-PGK. **a.** CD-spectra in absence and presence of urea; **b.** Unfolding curves, determined from the CD-signal $[\theta]$ at 222 nm, normalized to the signal at 0 M urea, against urea activity (for comparison, the lower abscissa shows urea concentration); solid lines are fits of the data to a two-state model, see text.

Appendix III: Simulations of Geminate Recombination Time Dependence

In our experiments, we followed the geminate recombination of thiyl radicals bound to a polypeptide backbone after they were created using short UV laser pulses. The relative motion of polypeptide-bound radicals, which is reflected in their recombination dynamics, is governed by the underlying motion/structural changes of the polypeptide. In the following, we present simulations which support our conclusion that the observed time dependence of the thiyl radical geminate recombination indicates subdiffusional behavior of the polypeptide sections to which the radicals are bound (intraprotein subdiffusion). The unusual recombination behavior is best seen in the time dependence of the instantaneous recombination rate constant, $k_{inst}(t) = -(dc/dt)/c$, where c is the thiyl radical concentration, which follows a power law of $t^{-0.94}$ over 9 orders of magnitude in time (from the picosecond to the millisecond time scale), see Figure 4.

In section 1, we show that normal diffusional behavior of the polypeptide sections to which the radicals are bound, diffusing either freely (section 1.1) or in a harmonic potential which approximates the tethering effect of the linking polymer chain (section 1.2), is not compatible with the observed power law behavior of $k_{inst}(t)$. This leads to the conclusion that the dynamic properties of the backbone significantly affect the motion of the polypeptide sections, and thus the recombination dynamics of the thiyl radicals, beyond the trivial tethering effect. In turn, this also means that the experimentally observed recombination dynamics contains information on the structural relaxation of the polypeptide backbone.

In section 2, we attempt to include the dynamic nature of the polymer backbone into the simulation, using different models, namely the free-draining and non-draining Rouse models (section 2.1), and the worm-like chain model which accounts for chain stiffness and excluded volume effects (section 2.2). Although these models modify the simulated time dependence of $k_{inst}(t)$, none of them can account for a power law of $t^{-0.94}$ over 9 orders of magnitude in time.

In section 3, we show that the observed recombination behavior is well described by subdiffusional motion of the polypeptide sections. These simulations are based on a continuous time random walk model with broad waiting time distribution which leads to a fractional diffusion equation and subdiffusive behavior, i.e. a mean square displacement that is nonlinear in time, $\langle r^2(t)\rangle \propto t^{\alpha}$ ($\alpha < 1$).

1. Simulations of Geminate Recombination Governed by Normal Diffusion

Diffusion of the radicals after their creation by a short UV pulse will be largely governed by the motion of the polypeptide sections to which they are bound. Recombination requires contact formation, followed by the actual chemical reaction. The dynamics of contact formation between reactive groups on a polypeptide, which is governed by intramolecular diffusion, has been investigated extensively using fluorescence or triplet quenching experiments, both for unstructured oligopeptides and small proteins (partially folded or unfolded) (3-17), single-molecule fluorescence correlation spectroscopy (18) or heme ligand binding following CO photodissociation (19, 20). Most of these experiments were analyzed assuming normal diffusion behavior, which gave reasonable agreement with experimental results and provided important insights into backbone dynamics. However, in all of these experiments the polypeptide backbone ensemble is in thermodynamic equilibrium before and during the experiment; in contrast, after disulfide photolysis the system is initially far from equilibrium and the results (especially the continuously decreasing instantaneous rate constant, Fig. 4) indicate that full equilibrium is not reached even on the maximum time scale of the experiment (1 ms).

The measured instantaneous rate constant for geminate recombination, $k_{inst}(t)$, is the ensemble-averaged probability of a reaction between two radicals. Its time dependence is governed by the diffusion-controlled probability of a re-encounter of the two radicals, multiplied by the probability of recombination upon contact formation before the radicals diffuse apart again. It decreases with time since the two reactants are initially in close vicinity but diffuse apart over time, reducing their chance of a re-encounter. However, the two radicals do not diffuse freely,

since they are tethered by the protein backbone, which prevents complete escape. Furthermore, the linking polypeptide backbone will modify the properties and time scale of diffusion.

Here, we simulate the expected time dependence of geminate radical recombination, which is controlled by diffusion of the polypeptide sections to which the radicals are bound, assuming "normal" diffusion (where the mean square displacement changes linearly in time: $\langle r^2 \rangle \sim t$), with the linking polypeptide backbone only affecting the effective diffusion constant ("free diffusion", section 1.1), or additionally taking into account its tethering effect (section 1.2); it will be shown that the experimentally observed power law, $k_{inst}(t) \propto t^{-0.94}$ over 9 orders of magnitude in time (1 ps to 1 ms), cannot be rationalized in this way.

1.1. Geminate Recombination of Radicals on Freely Diffusing Polypeptide Sections

1.1.1. Reencounter Probability for Non-Reacting Infinitely Small Particles

Assuming normal three-dimensional diffusion (random walk) with diffusion constant D, the probability density $p(r,t)$ of finding a (non-reacting) particle at distance r at time t, if the particle at $t = 0$ was at $r = 0$, is given by

$$p(r,t) = \frac{1}{8(\pi D t)^{1.5}} \exp\left(-\frac{r^2}{4Dt}\right) \tag{S1}$$

The probability that two radicals (assumed to be infinitely small), bound to different polypeptide sections and created at $t = 0$ in very close contact, will encounter each other again can be calculated by assuming that one radical remains fixed at the origin whereas the other one diffuses with a diffusion constant D which is the sum of the individual self-diffusion constants. This yields an encounter probability time dependence of $p(0,t) \sim t^{-1.5}$, predicting $k_{inst}(t) \sim t^{-1.5}$.

However, this ignores several important aspects of geminate recombination. In particular, radicals are not created and do not react at zero centre-to-centre distance; furthermore, the recombination reaction, which only occurs in the radical encounter region, may lead to a distortion of the particle density near the origin.

1.1.2. Finite Initial Pair Separation and Contact Distance

It is straightforward to calculate the time dependence of the probability for two radicals to encounter each other at a contact distance σ after being created at an initial pair separation r_0. Again, this can be done by assuming that one particle remains fixed at a distance of r_0 from the origin, whereas the other, initially at the origin, diffuses with a relative (intrachain) diffusion constant D. Averaging $p(r,t)$, Eq. (S1), over all positions which are at distance σ from the "fixed" radical yields the corresponding encounter probability density:

$$p(t) = \frac{1}{(2\pi)^{1.5} r_0 \sigma \sqrt{2Dt}} \; e^{-\frac{r_0^2+\sigma^2}{4Dt}} \; \sinh\left(\frac{r_0 \sigma}{2Dt}\right) \tag{S2}$$

The contact distance σ for aromatic thiyl radicals has been estimated to be 7.2 Å (21, 22). Geminate recombination in our experiments is found to start essentially immediately after radical pair generation, indicating that the initial pair separation r_0 cannot be significantly larger than σ; most likely, this is due to caging by the solvent and the protein which prevent significant separation during photolysis; a similar effect has been observed for model disulfides in high viscosity solvents (22). Therefore, we use values of r_0 in our simulations which are at most slightly larger than σ. The relative diffusion constant of polypeptide chain segments has been reported, mostly from fluorescence or triplet quenching experiments, to be on the order of 1-20 Å^2/ns, in the absence or presence of significant concentrations of denaturant, measured on unstructured oligopeptides or unfolded proteins (4, 6, 12, 19, 20, 23-26).

Figure S2 shows the time dependent encounter probability density at contact distance calculated from Eq. (S2) for a range of parameters (D, r_0 and σ). In all cases, the same general behavior is

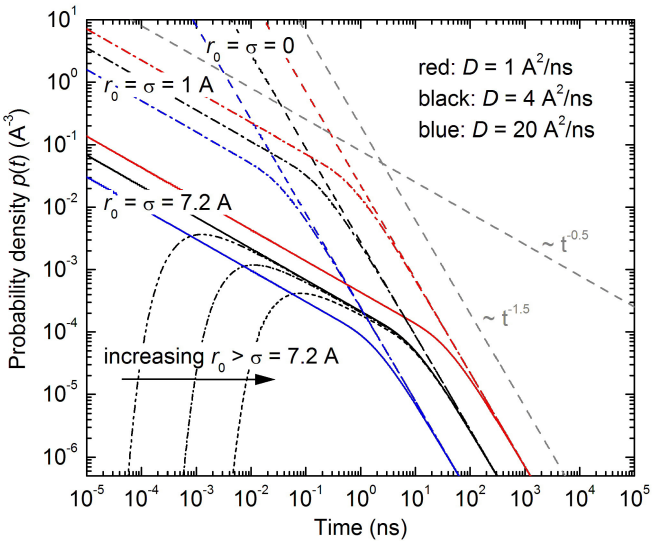

Figure S2. Time dependent encounter probability density at contact distance for (non-reacting) radicals, calculated from Eq. (S2) for a range of parameters: D = 1 Å^2/ns (red lines), 4 Å^2/ns (black lines) and 20 Å^2/ns (blue lines); $r_0 = \sigma = 0$ (dashed lines, results identical to Eq. (S1)), $r_0 = \sigma = 1$ Å (dash-dotted lines), $r_0 = \sigma = 7.2$ Å (solid lines). Also shown are results for D = 4 Å^2/ns, $\sigma = 7.2$ Å, and $r_0 = 7.3$ Å, 7.5 Å and $r_0 = 8$ Å. The grey dashed lines indicate power laws $t^{-0.5}$ and $t^{-1.5}$, respectively.

found. For $r_0 = \sigma > 0$ the probability density of re-encounter shows an initial decay $\sim t^{-0.5}$ at short times ($t << \tau_0 = r_0^2/D$), during which the average radical pair separation has not increased far beyond the initial separation r_0. At longer times, at which diffusion has gone well beyond the initial separation, this turns into a $\sim t^{-1.5}$ behavior, with the transition between the two regimes lasting not longer than one order of magnitude in time. For $r_0 > \sigma$, i.e. if the radicals are created at a separation which is larger than their encounter distance, there is an initial delay before any encounters can occur, corresponding to the time required for the radicals to diffuse over their initial separation distance ($\sim(r_0-\sigma)^2/D$).

Thus, several regions of the time-dependence of the reencounter probability of the two radicals/polypeptide sections are expected: (i) increasing probability, if the initial pair separation is larger than the contact distance, (ii) $\sim t^{-0.5}$ while $t < \sigma^2/D$, and finally (iii) $\sim t^{-1.5}$, once radicals have diffused over a distance larger than the contact distance. The transition between each of these regions is fast (less than an order of magnitude in time).

1.1.3. Survival Probability and Instantaneous Rate Constant of Geminate Recombination

It is also possible to take into account the distortion of the particle density near the encounter distance due to geminate recombination. Geminate recombination governed by free diffusion under these conditions has been studied extensively. A re-encounter at the contact distance σ leads to recombination with a probability which is described by a second-order rate coefficient, k_{rec}, and which is included into the diffusion equation via suitable boundary conditions. Ultimately, all geminate molecular pairs created at $t = 0$ will either have recombined or escaped from each other. The pair survival probability $P(t)$ at time t after pair creation is given by (27)

$$P(t) = 1 - \frac{\lambda}{\kappa(1+\lambda)}\left\{\operatorname{erfc}\left[\frac{\kappa - 1}{2\sqrt{t/\tau_0}}\right] - e^{(1+\lambda)(\kappa-1)}\, e^{(1+\lambda)^2(t/\tau_0)} \times \right. \qquad \text{(S3)}$$

$$\left. \times \operatorname{erfc}\left[(1+\lambda)\sqrt{t/\tau_0} + \frac{\kappa - 1}{2\sqrt{t/\tau_0}}\right]\right\}$$

where $\kappa = r_0/\sigma$, $\lambda = k_{rec}/k_D$, $k_D = 4\pi\sigma D$, and $\tau_0 = \sigma^2/D$ is the time constant for diffusion over the contact distance; erfc(x) is the complementary error function.

This equation has been shown to well describe the experimentally observed geminate recombination of aromatic thiyl radicals in solution (21, 22). The value of the recombination rate constant k_{rec} for aminophenyl thiyl radicals depends critically on the polarity of the solvent due to internal charge transfer between the amino group and the sulfur atom (28, 29). Values of k_{rec} of the order 10^{12} $cm^3mol^{-1}s^{-1}$ yield reasonable agreement between our experimental and simulated values for $k_{inst}(t)$, assuming a value of 1-20 $Å^2$/ns for D (see above); this compares well with values for k_{rec} reported for model aminophenyl thiyl recombination (22). It has to be noted that aminophenyl thiyl radicals are strongly stabilized against recombination in polar solvents by internal charge transfer (22, 30-32).

Figure S3a shows the expected effects for the time-dependent radical survival probability: slower diffusion leads to faster geminate recombination with higher overall recombination yield (red vs. black vs. blue solid lines), since the radicals are more likely to re-encounter each other and recombine before they diffuse apart. A smaller recombination rate constant (grey solid line), has the opposite effect. Finally, if the radicals are created at slightly larger initial separation, there is a delayed onset of recombination and a somewhat increased probability of cage escape.

The instantaneous rate constant $k_{inst}(t) = -(dP(t)/dt)/P(t)$ was calculated from Eq. (S3) for a wide

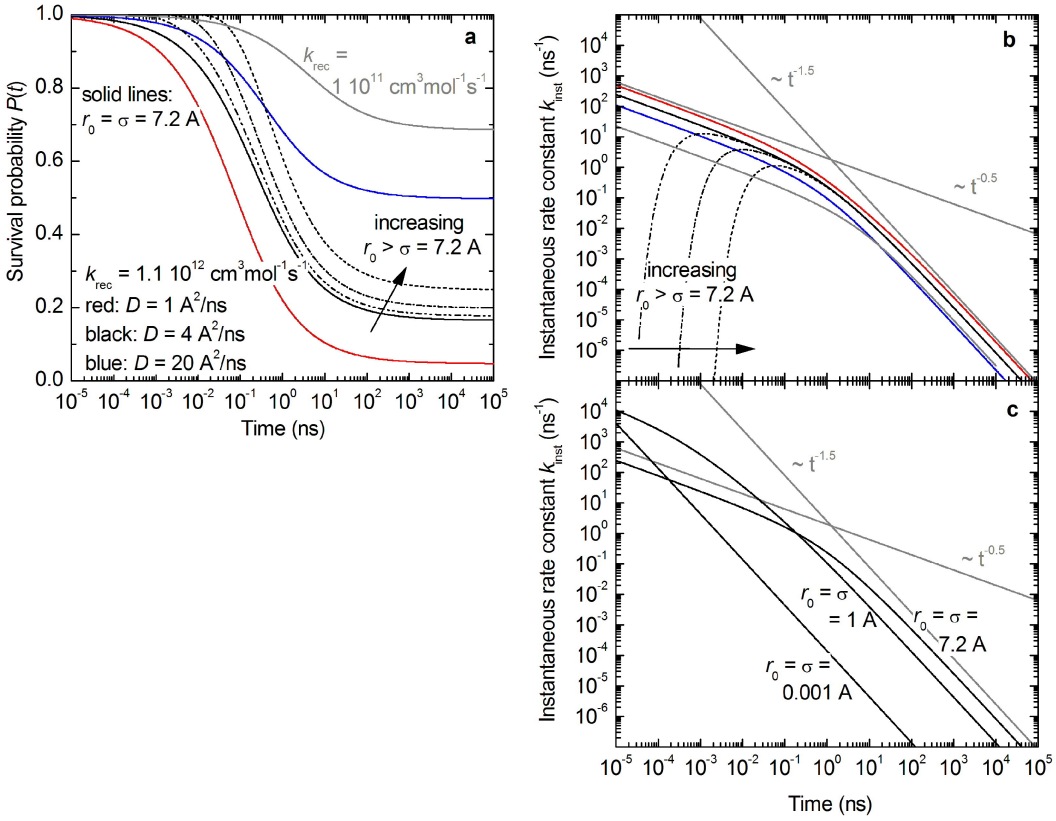

Figure S3. Time dependent survival probability (**a**) and resulting instantaneous rate constant of geminate recombination, $k_{inst} = -(dP(t)/dt)/P(t)$, (**b**, **c**) calculated from Eq. (S3) for a radical pair with encounter distance σ, initial pair separation r_0 and relative diffusion coefficient D recombining on encounter with a recombination rate coefficient k_{rec}. **a**, **b**: σ= 7.2 Å; D = 1 $Å^2$/ns (red line), 4 $Å^2$/ns (black and grey lines) and 20 $Å^2$/ns (blue line); r_0 = 7.2 Å (solid line), 7.3 Å (dash-dot-doted line), 7.5 Å (short dash-dotted line) and 8 Å (short dashed line); k_{rec} = 1.1 10^{12} $cm^3mol^{-1}s^{-1}$ (black, red, and blue lines) and 1.1 10^{12} $cm^3mol^{-1}s^{-1}$ (grey line). **c**: effect of varying r_0 and σ on the time dependence of k_{inst} for D = 4 $Å^2$/ns and k_{rec} = 1.1 10^{12} $cm^3mol^{-1}s^{-1}$. The grey dashed lines in **b** and **c** indicate power laws $t^{-0.5}$ and $t^{-1..5}$, respectively.

range of parameters, only a few are shown in Figures S3b and c. The time dependence of $k_{inst}(t)$ shows essentially the same behavior as that of the encounter probability density, Figure S2; for $r_0 > \sigma$, there is a delay before recombination starts, since the radicals first need to diffuse together. Following this initial delay, $k_{inst}(t)$ decays $\sim t^{-0.5}$ for short times, whereas at longer times it proceeds $\sim t^{-1.5}$. The transition between the two regimes spans at most a few orders of magnitude in time. This shows that under the conditions prevailing for recombination of aromatic thiyl radicals on polypeptide side chains, the time dependence of $k_{inst}(t)$ is essentially governed by the time dependent encounter probability calculated from diffusion in the absence of recombination; only minor effects are introduced by the local distortion of the particle density near the encounter distance due to recombination. This is due to the small intrinsic recombination rate constant of aminophenyl thiyl radicals, which results in a non-diffusion controlled reaction (22, 30-32). For some of the models described below, it will not be possible to explicitly calculate the instantaneous recombination rate constant, but only the time-dependent probability density for radical re-encounters in the absence of recombination; in these cases, we will make use of this similarity in the time dependence of these two quantities.

In summary, we conclude that free diffusion of the peptide ends is not able to account for the experimentally found uniform power law for the decay of the instantaneous recombination rate constant $k_{inst}(t) \sim t^{-0.94}$ over 9 order of magnitude in time.

1.2. Geminate Recombination of Tethered Radicals

Eq. (S3) does not include the tethering effect of the polypeptide chain which links the two residues to which the radicals are bound. Although many authors have treated diffusion-controlled intrachain polymer reactions theoretically (33-39), often in the context of quenching or ring closure experiments, all of these treatments assume an initial fully equilibrated configurational ensemble and are therefore not applicable to the geminate recombination problem encountered here. Therefore, a series of simulations were performed to investigate the effects of the tether on geminate recombination dynamics. Following previous approaches to the tethering problem, these simulations model the effect of the tether by assuming that the radicals diffuse in a harmonic potential (33, 37) which allows for virtually free diffusion at short radical distances, but introduces an increasing energy penalty when the radicals separate to larger distances, resulting in the Gaussian distribution of the end-to-end distance expected for a random coil tether. Thus, the potential energy at radical-radical distance r, $U_{harm}(r)$, is given by

$$U_{\mathrm{harm}}(r) = \frac{3k_{\mathrm{B}}T}{2L^2} r^2 \qquad \text{(S4)}$$

where L is the root mean square distance of the radicals in equilibrium, k_B is the Boltzmann constant and T the temperature. The root mean square end-to-end distance of an unfolded polypeptide with N residues has a typical value given by $L^2 \approx c_N N a^2$, where a is the C^{α}-C^{α}-distance (3.8 Å) and c_N is Flory's characteristic ratio, which accounts for chain stiffness/ persistence length effects and has a typical value of 7-10, depending on composition and length of the polypeptide (5, 8, 19, 20, 24, 40, 41). Similar values have been reported in the absence and presence of denaturant, although indirect evidence exists showing that the addition of denaturant can lead to an increase of L (24). The segment of polypeptide backbone connecting the radicals consists of 11 residues in N-PGK and of 17 residues in the model peptide studied by Volk *et al* (31), predicting values for L on the order of 35 Å and 45 Å, respectively.[†] For fully exploring the effects, values between 15 and 100 Å were used for simulations, although only results for 25 Å and 45 Å are shown; simulations using other values did not yield any significantly different results, except for the expected change of the time at which

[†] For the model peptides studied by Volk *et al* (31), this corresponds to the full length of the peptide. For N-PGK, the backbone sections on either side of the loop formed by the disulfide bond cross-link will to some extent modify the dynamic behavior, but this can be accounted for by changing the effective diffusion constant (7). Since the simulations performed here are not aimed at providing an exact quantitative comparison with experimental data, this does not affect our conclusions.

conformational equilibration is reached, which leads to a leveling off of the re-encounter probability or the instantaneous rate constant, see below.

In the following, we first calculate the reencounter probability for two infinitely small radicals created at the origin and diffusing in a harmonic potential (i.e. tethered); next, the equations for two radicals making contact at a contact distance σ after being created at an initial pair separation r_0 will be derived; finally, we will present numerical simulation results of the same problem including a finite reaction probability at the encounter distance.

1.2.1. Reencounter Probability for Non-Reacting Infinitely Small Particles

The probability density $p(\boldsymbol{x},t)$ of finding a particle at position $\boldsymbol{x}$ at time t, whose motion is governed by diffusion in a potential $U(\boldsymbol{x})$, is given by the Smoluchowski equation (33, 37)

$$\frac{\partial}{\partial t} p(\boldsymbol{x},t) = D\nabla\left(\nabla p(\boldsymbol{x},t) + p(\boldsymbol{x},t)\nabla U(\boldsymbol{x})/kT\right) \tag{S5}$$

Making use of the starting condition that the particle at $t = 0$ is at $r = 0$, i.e. $p(r,t=0) = \delta(r)$, and the spherical symmetry of the problem, it is straightforward to derive the solution of this equation for the harmonic potential, $U_{\text{harm}}(r)$:

$$p(r,t) = \frac{1}{(2\pi\, g(t))^{1.5}} e^{-\frac{r^2}{2g(t)}}$$

with (S6)

$$g(t) = \frac{L^2}{3}\left(1 - e^{-\frac{6Dt}{L^2}}\right)$$

As expected, this reduces to Eq. (S1) for $Dt << L^2$, i.e. for a long tether or for short times.

Again, this equation can be used for calculating the re-encounter probability of two radicals by assuming that one radical remains fixed at the origin whereas the other one diffuses with a relative diffusion constant D. As shown in Figure S4, this re-encounter probability $p(r=0,t)$ for infinitely small particles initially decreases ~ $t^{-1.5}$, just as in the case of free diffusion. Only at times of the order $t \sim L^2/D$, i.e. when diffusion has taken place over the length scale of the potential/tether, does $p(0,t)$ show any deviation from free diffusion. On this time scale, the system reaches its equilibrium conformational distribution, and $p(0,t)$ becomes time-independent. The transition between the two regions occurs within one order of magnitude in time.

1.2.2. Finite Initial Pair Separation and Contact Distance

Diffusion of two radicals in a harmonic potential is governed by Eq. (S5). In this case, the reduced Green function, $G(\boldsymbol{u}_1,\boldsymbol{u}_2,t)$, which describes the probability that the radical separation vector $(\boldsymbol{r}_2 - \boldsymbol{r}_1)$ is given by $\boldsymbol{u}_2$ at time t if it was $\boldsymbol{u}_1$ at time $t = 0$ (averaging over all equilibrium polymer configurations with $(\boldsymbol{r}_2 - \boldsymbol{r}_1) = \boldsymbol{u}_1$), has the following form (35):

$$G(\boldsymbol{u}_1,\boldsymbol{u}_2,t) = \frac{\left(1-\rho^2(t)\right)^{1.5}}{(2\pi\, g(t))^3} e^{-\frac{\boldsymbol{u}_1^2 - 2\rho(t)\boldsymbol{u}_1\cdot\boldsymbol{u}_2 + \boldsymbol{u}_2^2}{2g(t)}}$$

with (S7)

$$g(t) = \frac{L^2}{3}\left(1-\rho^2(t)\right)$$

$$\rho(t) = e^{-\frac{3Dt}{L^2}}$$

where $\rho(t)$ is the normalized time correlation function of the polymer end-to-end vector, here approximated by a single harmonic spring connecting the ends.

Calculating the re-encounter probability of two (non-reacting) radicals at a contact distance σ after being created at an initial pair separation r_0 (in the absence of recombination) requires averaging $\boldsymbol{u}_1$ over all polypeptide backbone conformations giving an initial pair separation r_0 and integrating $\boldsymbol{u}_2$ over all conformations corresponding to a distance σ, which yields:[‡]

$$p(t) = \frac{1}{(2\pi)^{1.5} r_0 \sigma \rho(t) \sqrt{g(t)}} e^{-\frac{r_0^2 \rho^2(t) + \sigma^2}{2g(t)}} \sinh\left(\frac{r_0 \sigma \rho(t)}{g(t)}\right) \tag{S8}$$

As expected, this equation reduces to Eq. (S2) for $Dt \ll L^2$, i.e. for a long tether or for short times. This is shown exemplary in Figure S4, where solid lines show results obtained for $r_0 = \sigma$ = 7.2 Å with Eq. (S8), i.e. in the presence of a harmonic potential, and dotted lines show results for the same conditions obtained with Eq. (S2), i.e. in the absence of a tether.

In general, for short times, during which the radicals have not yet had sufficient time for diffusion over the length scale of the tether, the results obtained with Eqs. (S2) and (S8) are identical. After this time, the tethered radicals assume their conformational equilibrium, yielding a time-independent re-encounter probability. The transition between these regions occurs in less than one order of magnitude in time.

Thus, in the presence of a tether, several regions of the time-dependent behavior of the reencounter probability of the two radicals are expected: (i) increasing probability, if the initial pair separation r_0 is larger than the contact distance σ, (ii) ~ $t^{-0.5}$ until $t \approx \sigma^2/D$, (iii) ~ $t^{-1.5}$ until $t \approx L^2/D$, and (iv) independent of time once conformational equilibrium has been attained. Each transition between these different regions is fast (less than one order of magnitude in time).

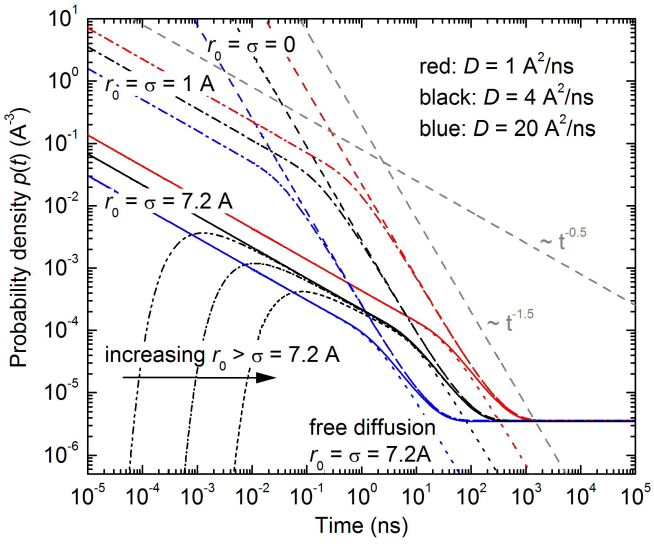

Figure S4. Time dependent encounter probability density at contact distance for (non-reacting) radicals undergoing diffusion in a harmonic potential with L = 45 Å, calculated from Eq. (S8) for a range of parameters: D = 1 Å^2/ns (red lines), 4 Å^2/ns (black lines) and 20 Å^2/ns (blue lines); $r_0 = \sigma = 0$ (dashed lines, results identical to Eq. (S6)), $r_0 = \sigma = 1$ Å (dash-dotted lines), $r_0 = \sigma = 7.2$ Å (solid lines). Also shown are results for D = 4 Å^2/ns, $\sigma = 7.2$ Å, and r_0 = 7.3 Å, 7.5 Å and r_0 = 8 Å. The dotted lines show the results in the absence of a harmonic potential for $r_0 = \sigma = 7.2$ Å. The grey dashed lines indicate power laws $t^{-0.5}$ and $t^{-1.5}$, respectively.

[‡] It has to be noted that here, as already for the derivation of Eq. (S7), a random coil equilibrium distribution of the polymer backbone was assumed, i.e. any partial folding of the backbone was ignored.

1.2.3. Survival Probability and Instantaneous Rate Constant

While the survival probability of a freely diffusing reactant pair undergoing geminate recombination can be calculated explicitly, Eq. (S3), to the best of our knowledge no analytic solution is available for reactants diffusing in a harmonic potential. We therefore simulated the effects of a reaction at contact distance σ numerically. For this purpose, a sink term was added to the diffusion equation, Eq. (S5), which describes a reaction at distance σ with rate constant k_{rec}:

$$\frac{\partial}{\partial t} p(r,t) = D\nabla\left(\nabla p(r,t) + p(r,t)\nabla U(r)/kT\right) - k_{rec}\delta(r-\sigma)p(r,t) \qquad \text{(S9)}$$

The harmonic potential, $U_{harm}(r)$, of Eq. (S4) was used for $U(r)$. The numerical simulations, starting from the initial condition $p(r,t=0) = \delta(r-r_0)$, included reflecting boundary conditions at $r = \sigma$ and at the outer limit of the simulation volume (with a radius of typ. 200 Å) and were implemented in MathCad, using the kinetic matrix method (4, 42, 43). The survival probability at time t, $P(t)$, is calculated by integrating the probability density $p(r,t)$ over the whole volume.

Simulations were run for a wide range of values for all parameters, and the same general behavior was obtained in all cases. As expected, the time dependence of Eq. (S3) was obtained for short times, see Figure S5a. Only on the timescale of $\sim L^2/D$, on which radicals diffuse over the length scale of the potential/tether, do any significant deviations appear. Unlike freely diffusing radicals, which can escape and thus avoid geminate recombination completely, all tethered radicals will eventually recombine, and thus their survival probability will drop to zero, see Figure S5a. The same behavior is seen in the instantaneous rate constant for recombination, $k_{inst}(t) = -(dP(t)/dt)/P(t)$, Figures S5b and c. The time dependence of $k_{inst}(t)$ is identical to that calculated in the absence of a potential up to times corresponding to the diffusion over length scale L. Only on this time scale will the radicals diffuse sufficiently far to encounter the effects of the harmonic potential. At this point, within one order of magnitude in time, conformational equilibrium is achieved, resulting in leveling off of $k_{inst}(t)$.

Thus, even in the presence of a tether $k_{inst}(t)$ is expected to rise initially, at least if photolysis leads to separation of the radicals beyond the contact distance. Subsequently, $k_{inst}(t)$ is expected to decay $\sim t^{-0.5}$, followed by a phase with a decay $\sim t^{-1.5}$, until it becomes independent of time once diffusion has lead to conformational equilibration, which is expected to occur on the time scale of 100 ns to a few µs. This is in stark contrast to the experimentally observed power law of $t^{-0.94}$ over 9 orders of magnitude in time (from the picosecond to the millisecond time scale), so that we conclude that the radicals do not follow a normal diffusive behavior. Again, these simulation also show that the time dependence of the instantaneous rate constant reflects that of the encounter probability, i.e. that the distortion of the particle density near the origin by the recombination reaction does not significantly affect the overall reaction behavior.

2. Effect of Polymeric Nature of Polypeptide Tether

The results described in section 1.2 only account for the tethering effect of the polypeptide backbone, but ignore its internal dynamics. Two models describing different aspects of the internal polypeptide structure on its dynamics, the Rouse model and the wormlike chain model, have been used to test if these could provide an explanation for the observed power law of the decay of the instantaneous rate constant $k_{inst}(t)$. It will be shown that neither of these models yields the experimentally observed power law of $t^{-0.94}$ over 9 orders of magnitude in time.

2.1. Rouse Model

Internal polymer dynamics have been successfully described using the Rouse (44) or Rouse-Zimm (45) models, often referred to as the free- and non-draining Rouse chain, respectively. These models assume the polymer to consist of a number of N_R beads connected by harmonic springs, yielding N_R-1 normal modes.[§] Whereas in the free-draining Rouse model, each bead

[§] N_R does not correspond to the number of residues, N, but more realistically is given by N/c_N, where c_N is Flory's characteristic ratio, which accounts for chain stiffness/persistence length effects, see above.

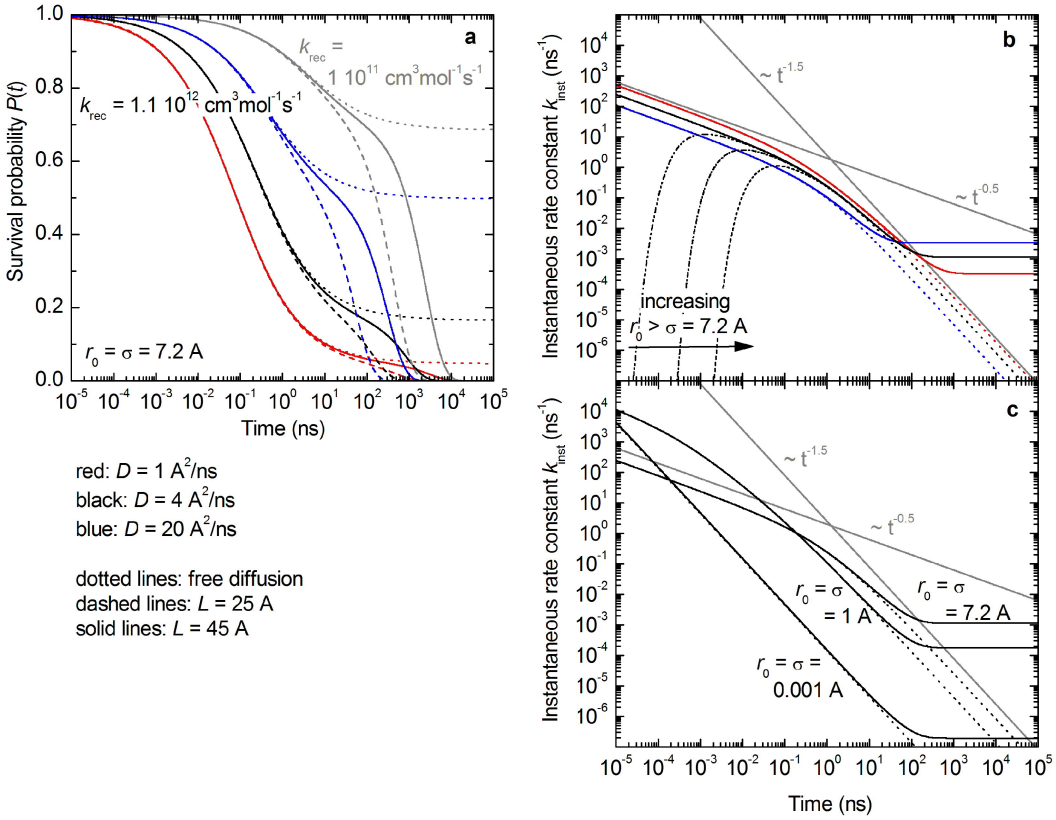

Figure S5. Time dependent survival probability (**a**) and resulting instantaneous rate constant of geminate recombination, $k_{inst} = -(dP(t)/dt)/P(t)$, (**b**, **c**) for tethered radicals, approximated by diffusion in a harmonic potential, Eq. (S4), with L = 45 Å (solid lines) or 25 Å (dashed lines), calculated from the numerical simulations described in the text. For comparison, also included are the results for free diffusion (Eqs. (S3), dotted lines). Shown are the results for a radical pair with encounter distance σ, initial pair separation r_0 and relative diffusion coefficient D recombining on encounter with a recombination rate coefficient k_{rec} with the following values: **a**, **b**: $r_0 = \sigma$= 7.2 Å; D = 1 Å^2/ns (red lines), 4 Å^2/ns (black and grey lines) and 20 Å^2/ns (blue lines); k_{rec} = 1.1 10^{12} cm^{3}mol^{-1}s^{-1} (black, red, and blue lines). **a**: also included are the results for k_{rec} = 1 10^{11} cm^{3}mol^{-1}s^{-1} (grey). **b**: also included are results for r_0 = 7.3 Å, 7.5 Å and 8 Å; **c**: effect of varying r_0 and σ on the time dependence of k_{inst} for D = 4 Å^2/ns and k_{rec} = 1.1 10^{12} cm^{3}mol^{-1}s^{-1}. The grey dashed lines in **b** and **c** indicate power laws t$^{-0.5}$ and t$^{-1..5}$.

experiences solvent friction which is independent of the motion of the other beads, the more realistic non-draining Rouse model also accounts for hydrodynamic interactions between beads, i.e. the "drag" experienced by a section of the polymer because of motion of the other sections.

For these models, the normalized time correlation function of the polymer end-to-end vector, $\rho(t)$, can be given by (35)

$$\rho_{Rouse}(t) = \frac{8}{\pi^2} \sum_{p;\text{odd}} p^{-2} \exp(-\lambda_p t)$$

with (S10)

$$\lambda_p = p^2 / \tau_m \quad \text{(free - draining Rouse chain)}$$
$$\lambda_p = p^{1.5} / \tau_m \quad \text{(non - draining Rouse chain)}$$

where the maximum relaxation time is given by $\tau_m = fN^2a^2/(3\pi^2 k_B T)$, f is the segmental friction coefficient, N the number of residues, a the length of a residue, k_B the Boltzmann constant and T

the temperature. With the Stokes-Einstein relation, $D = k_B T/f$, and the root mean square end-to-end distance L given above, $L^2 \approx c_N N a^2$, this becomes $\tau_m = N/(\pi^2 c_N) * L^2/3D$. For the sake of simplicity, however, here we used the same value of τ_m, the longest relaxation time, as was used for the relaxation time in the single harmonic spring model, i.e. $\tau_m = L^2/3D$, see Eq. (S7), which overestimates the value of τ_m by a factor of 2-4. It has to be noted that no quantitative, but only qualitative simulations were attempted here and that the value of D, and consequently of τ_m, was varied over a wide range with no change in the general behavior.

The reencounter probability of two radicals at contact distance σ after being created at an initial pair separation r_0 (in the absence of recombination) in the free- or non-draining Rouse model was calculated using Eq. (S8) with $\rho(t)$ from Eq. (S10). Figures S6a and S7a show simulations where summation over p was performed to convergence, which corresponds to modeling very long polymer chains with unrealistically small beads. Figures S6b-d and S7b-d compare the results of assuming a smaller number of larger beads, corresponding to the same polymer length; this situation was approximated by summing over less terms in Eq. (S10).

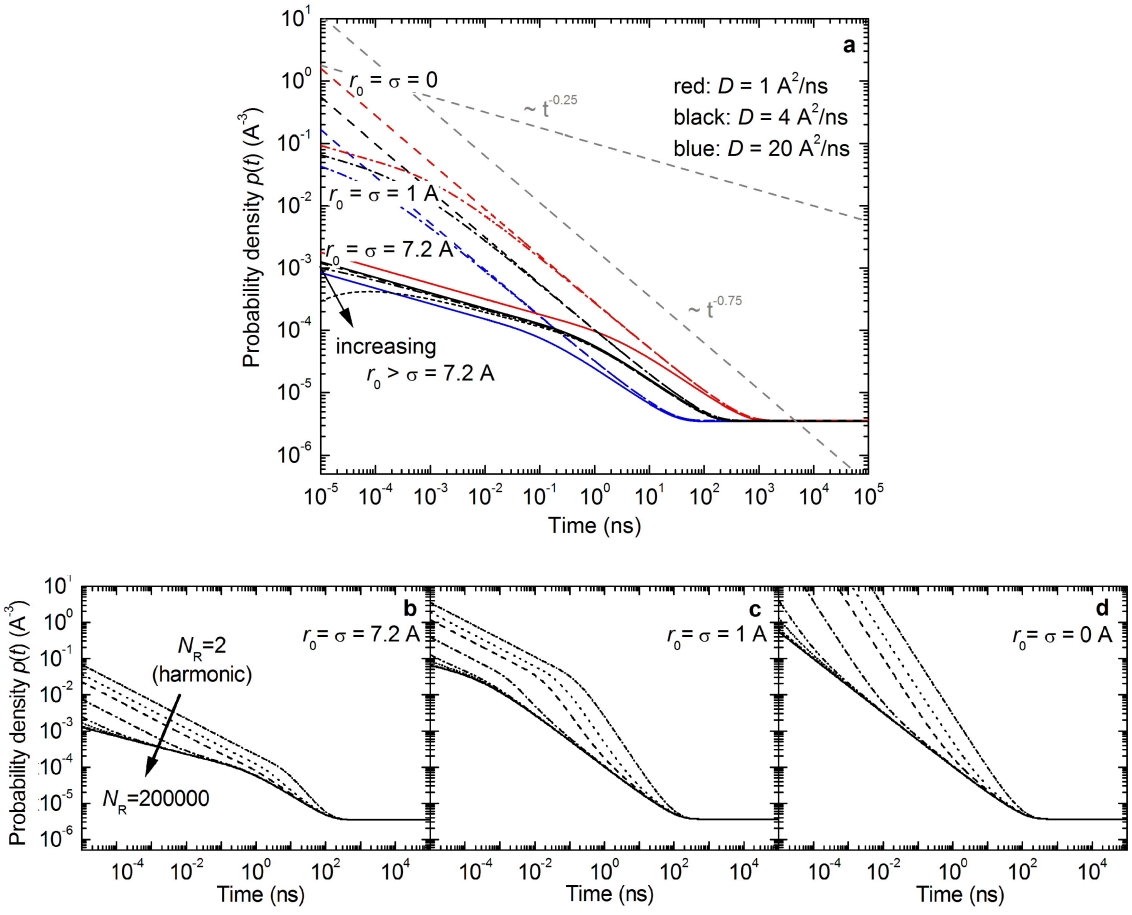

Figure S6. Time dependent encounter probability density at contact distance for (non-reacting) radicals at the end of a free-draining Rouse chain, calculated from Eqs. (S8) and (S10); τ_m was assumed to be given by $L^2/3D$, with $L = 45$ Å. **a.** Simulations with summation over p performed to convergence (very long polymer chains consisting of small beads), for a range of parameters: D = 1 Å^2/ns (red lines), 4 Å^2/ns (black lines) and 20 Å^2/ns (blue lines); $r_0 = \sigma = 0$ (dashed lines), $r_0 = \sigma = 1$ Å (dash-dotted lines), $r_0 = \sigma = 7.2$ Å (solid lines). Also shown are results for D = 4 Å^2/ns, $\sigma = 7.2$ Å, and r_0 = 7.3 Å, 7.5 Å and r_0 = 8 Å. The grey dashed lines indicate power laws $t^{-0.25}$ and $t^{-0.75}$, respectively. **b-d.** Effect of assuming a smaller number (N_R) of larger beads for D = 4 Å^2/ns; $N_R = 2$ corresponds to diffusion in a harmonic potential and yields the same results as shown in Fig. S4.

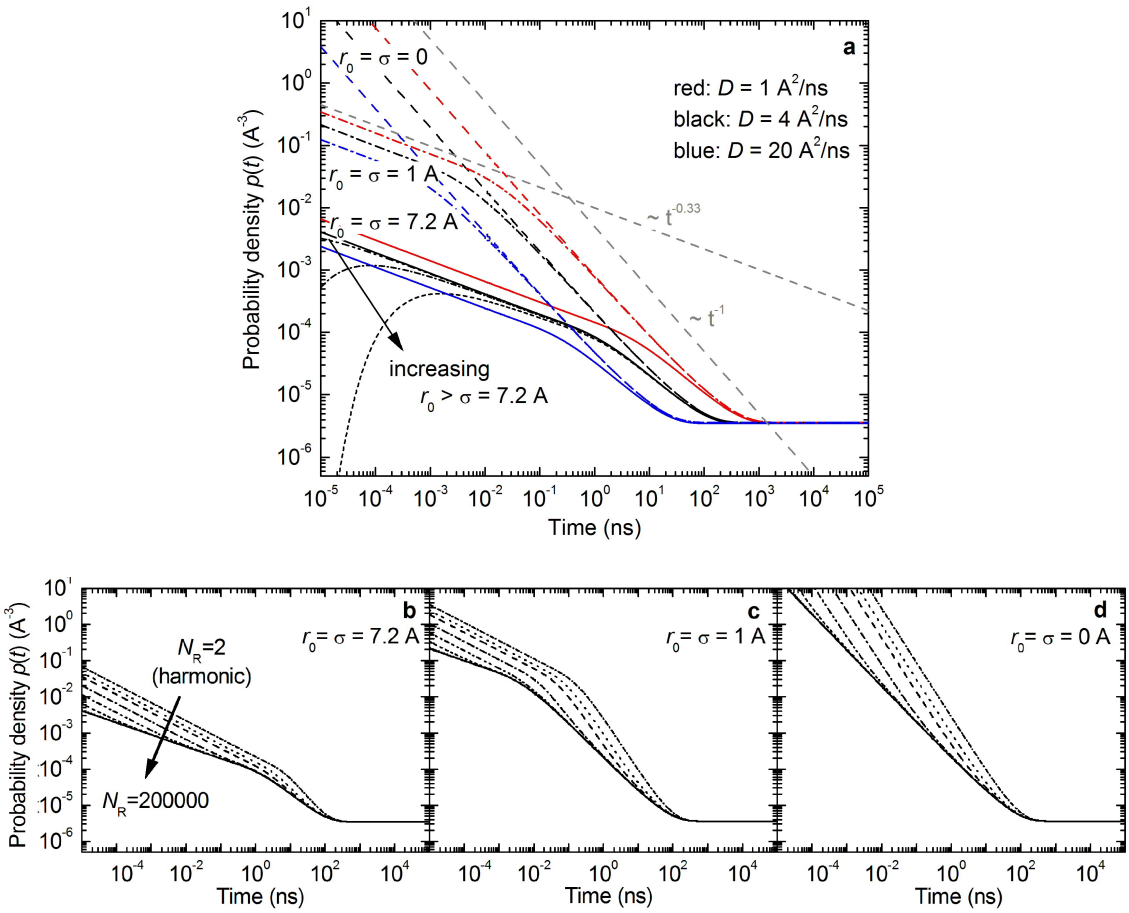

Figure S7. Time dependent encounter probability density at contact distance for (non-reacting) radicals at the end of a non-draining Rouse chain, calculated from Eqs. (S8) and (S10); τ_m was assumed to be given by $L^2/3D$, with L = 45 Å. **a.** Simulations with summation over p performed to convergence (very long polymer chains consisting of small beads), for a range of parameters: D = 1 Å^2/ns (red lines), 4 Å^2/ns (black lines) and 20 Å^2/ns (blue lines); $r_0 = \sigma = 0$ (dashed lines), $r_0 = \sigma = 1$ Å (dash-dotted lines), $r_0 = \sigma = 7.2$ Å (solid lines). Also shown are results for D = 4 Å^2/ns, σ= 7.2 Å, and r_0 = 7.3 Å, 7.5 Å and r_0 = 8 Å. The grey dashed lines indicate power laws $t^{-0.33}$ and t^{-1}, respectively. **b-d.** Effect of assuming a smaller number (N_R) of larger beads for D = 4 Å^2/ns; N_R = 2 corresponds to diffusion in a harmonic potential and yields the same results as shown in Fig. S4.

Figure S6a shows that the free-draining Rouse model for long polymers shows the same principal behavior of the radical encounter probability as the harmonic model, albeit with lower power laws; after an initial increase, which only is found if $r_0 > \sigma$, the encounter probability decays ~ $t^{-0.25}$ until diffusion has occurred over a length scale of σ,[**] at which point the behavior changes to ~ $t^{-0.75}$, until full equilibration occurs on the timescale of τ_m, when the encounter probability becomes time-independent. This slower decay of the encounter probability than that for free diffusion are in agreement with the well-known fact that in the Rouse model the peptide ends efficiently explore a compact space (38).

However, for shorter polymer chains this behavior only is found at times which are larger than the shortest relaxation time $\tau_m/(N_R\text{-}1)^2$, at shorter times the model predicts a behavior identical to that observed for the harmonic model, i.e. encounter probability decays ~ $t^{-0.5}$ and ~ $t^{-1.5}$

[**] It has to be noted that in the Rouse model, diffusion of the peptide ends does not follow the normal diffusion equation, and therefore the time scale of diffusion over a length scale σ is not given by σ^2/D.

before and after diffusion over length scale σ, respectively (Fig. S6 b-d). Thus, depending on the relative values of the shortest and longest relaxation times and the time for diffusion over the length scale of σ, a complex behavior can be observed, e.g. the decay of the encounter probability decaying initially ~ $t^{-0.5}$, followed by a period where it decays ~ $t^{-0.25}$, then changing to ~ $t^{-0.75}$, before it levels off, see in particular Figure 6b. In all cases, the transition between the different power laws is found to occur within one or two orders of magnitude in time.

The non-draining Rouse model (Fig. S7) yields similar results, except that for long polymers the encounter probability decays proportional to ~ $t^{-0.33}$ until diffusion has occurred over a length scale of σ, and ~ t^{-1} after that time, until it becomes time-independent when full equilibration occurs on the timescale of τ_m. Again, for shorter polymer chains this behavior only is found at times which are larger than the shortest relaxation time, $\tau_m/(N_R\text{-}1)^2$, at shorter times the model predicts a behavior identical to that observed for the harmonic model, i.e. encounter probability decays ~ $t^{-0.5}$ and ~ $t^{-1.5}$ before and after diffusion over length scale σ, respectively.

For the Rouse model, it was only possible to calculate the time dependence of the encounter probability in the absence of a reaction; however, it was shown above that this yields a good approximation of the general behavior of the instantaneous rate constant due to the low inherent recombination rate constant of aromatic amino-thiyl radicals. In no case (free- or non-draining; infinitely long or shorter polymer chain, wide range of input parameters) a power law ~ $t^{-0.94}$ was found to be predicted for the encounter probability over the full time scale used in the experiments (ps to ms). In particular for short chain lengths, which is a more realistic model for the protein investigated here or the model peptide investigated by Volk *et al* (31), a complex behavior is expected with the power law changing several times before the encounter probability becomes constant upon equilibration on the microsecond time scale. This is contrary to the experimentally found uniform power law ~ $t^{-0.94}$, over the full time range from picoseconds to milliseconds, which suggests that even a model that includes internal (Rouse) polymer dynamics does not account for the observed power law decay of the instantaneous rate constant over 9 orders of magnitude in time.

2.2. Chain Stiffness and Excluded Volume

Other important aspects of the diffusional behavior of the polypeptide backbone, in particular of short peptides or protein sections, are chain stiffness and excluded volume effects. Chain stiffness refers to the finite bending rigidity of the backbone, which propagates in the general direction of the initial section for several residues, the number of which is characterized by the persistence length l_p. For short peptides (with N residues), whose contour length $l_c = N * 3.8$ Å is on the order of l_p, this results in a significant non-Gaussian equilibrium distribution of the end-to-end distance (4), whereas no effect of chain stiffness is expected if $l_c >> l_p$. Excluded volume effects, on the other hand, are based on the trivial observation that the volume occupied by one residue is not available to other residues. This contributes to the finite bending rigidity of the polymer, since the chain is prevented from folding back on itself, but in addition has effects on the relative conformations of residues which are further apart than l_p (7).

For the non-equilibrium situation encountered during geminate thiyl radical recombination, it could be expected that these effects affect the encounter rate of radicals; this is particularly true if the radicals are linked by relatively short peptide sections, since conformations which require strong local backbone bending, i.e. those with a short end-to-end distance, are less likely to be adopted. Thus, *a priori* it cannot be ruled out that chain stiffness and/or excluded volume effects could cause the experimentally observed uniform power law decay $k_{inst}(t) \sim t^{-0.94}$ over 9 order of magnitude in time. To investigate this possibility, we undertook numerical simulations of the time-dependent survival probability and instantaneous radical recombination rate constant which take these effects into account.

For these simulation, we made use of analytical expressions for the end-to-end distance distribution $p_x(r)$ which have been derived in the literature, based on theoretical models, simulations (4, 7, 46, 47) or experimental results (13). From these distributions an effective

potential energy at distance r, $U_x(r)$, which describes the motion of the peptide ends and yields the correct equilibrium end-to-end distance distribution, can be calculated:[††]

$$U_x(r) = -kT \ln \frac{p_x(r)}{4\pi r^2} \tag{S11}$$

This potential was used in numerical simulations identical to those described in section 1.2.3, except for the use of $U_x(r)$ instead of the harmonic potential in the diffusion equation, Eq. (S9).

2.2.1. Chain Stiffness Effects

The equilibrium distribution $p_{cs}(r)$ of the end-to-end distance r for a polypeptide with persistence length l_p and contour length l_c can be simulated using the wormlike chain model originally developed by Porod and Kratky (48).

Based on this model, the following analytical expression for $p_{cs}(r)$ was derived for polymers with large bending rigidity (i.e. $l_p > l_c$) (47):

$$p_{cs}(r) = Nr^2 \frac{1}{(l_p(l_c - r))^{3/2}} \sum_{i=1}^{\infty} e^{-\frac{l_c^2 (i-0.5)^2}{l_p (l_c - r)}} \left(\frac{4 l_c^2 (i-0.5)^2}{l_p (l_c - r)} - 2 \right) \tag{S12}$$

For the opposite extreme case, i.e. very small bending rigidity (i.e. $l_p < l_c/10$), a different distribution was found (46):

$$p_{cs}(r) = 4\pi r^2 (0.75\pi l_p l_c)^{3/2} e^{-\frac{3r^2}{4 l_p l_c}} \left(1 - \frac{5 l_p}{4 l_c} + \frac{2r^2}{l_c^2} - \frac{33 r^4}{80 l_p l_c^3} - \frac{79 l_p^2}{160 l_c^2} - \frac{329 r^2 l_p}{120 l_c^3} + \frac{6799 r^4}{1600 l_c^4} - \frac{3441 r^6}{2800 l_p l_c^5} + \frac{1089 r^8}{12800 l_p^2 l_c^6} \right) \tag{S13}$$

For polypeptides, values in the range from 2 to 15 Å have been reported for the persistence length l_p based on a range of different experimental methods (4, 49-53). Thus, for the situation investigated here (N = 11 residues in the protein investigated here and 17 residues in the model peptide studied by Volk *et al* (31)), neither of these approximations is strictly valid.

Lapidus *et al* (4) reported an analytical expression for $p_{cs}(r)$ which interpolates between the distributions given in Eqs. (S12) and (S13), based on extensive numerical simulations of wormlike chains with values for l_c/l_p ranging from 1 to 10 (this expression is complex, and thus is not reproduced here). Using this equilibrium distribution, they determined a value of 6.4 Å for l_p from equilibrium triplet quenching data on short model peptides, which is comparable to the values ranging from 2 to 15 Å determined by other methods (49-53).

We used the effective potentials $U_{cs}(r)$, calculated from these analytical expressions for the end-to-end distributions using Eq. (S11), for numerically simulating the time-dependent survival probability and instantaneous recombination rate constant in the presence of chain stiffness effects, varying the parameter l_p over the range of values reported in the literature. Figure S8 shows typical results for the instantaneous rate constant $k_{inst}(t)$ obtained from these simulations and compares them to results obtained with the harmonic spring potential. It can be seen that at

---

[††] Note that the divisor $4\pi r^2$ is required since $p_x(r)$ is usually reported as the 1-dimensional distribution of the end-to-end distance, whereas Eq. (S9) is written in 3 dimensions. Eq. (S11) yields the harmonic potential of Eq. (S4) (except for an irrelevant constant offset) for the Gaussian distribution $p_{harm}(r) \propto 4\pi r^2 \exp(-3r^2/2L^2)$ of the freely jointed chain.

short times, the time dependence of $k_{inst}(t)$ is independent of the persistence length l_p and is identical to that obtained with a harmonic potential. As expected, $k_{inst}(t)$ levels off at longer

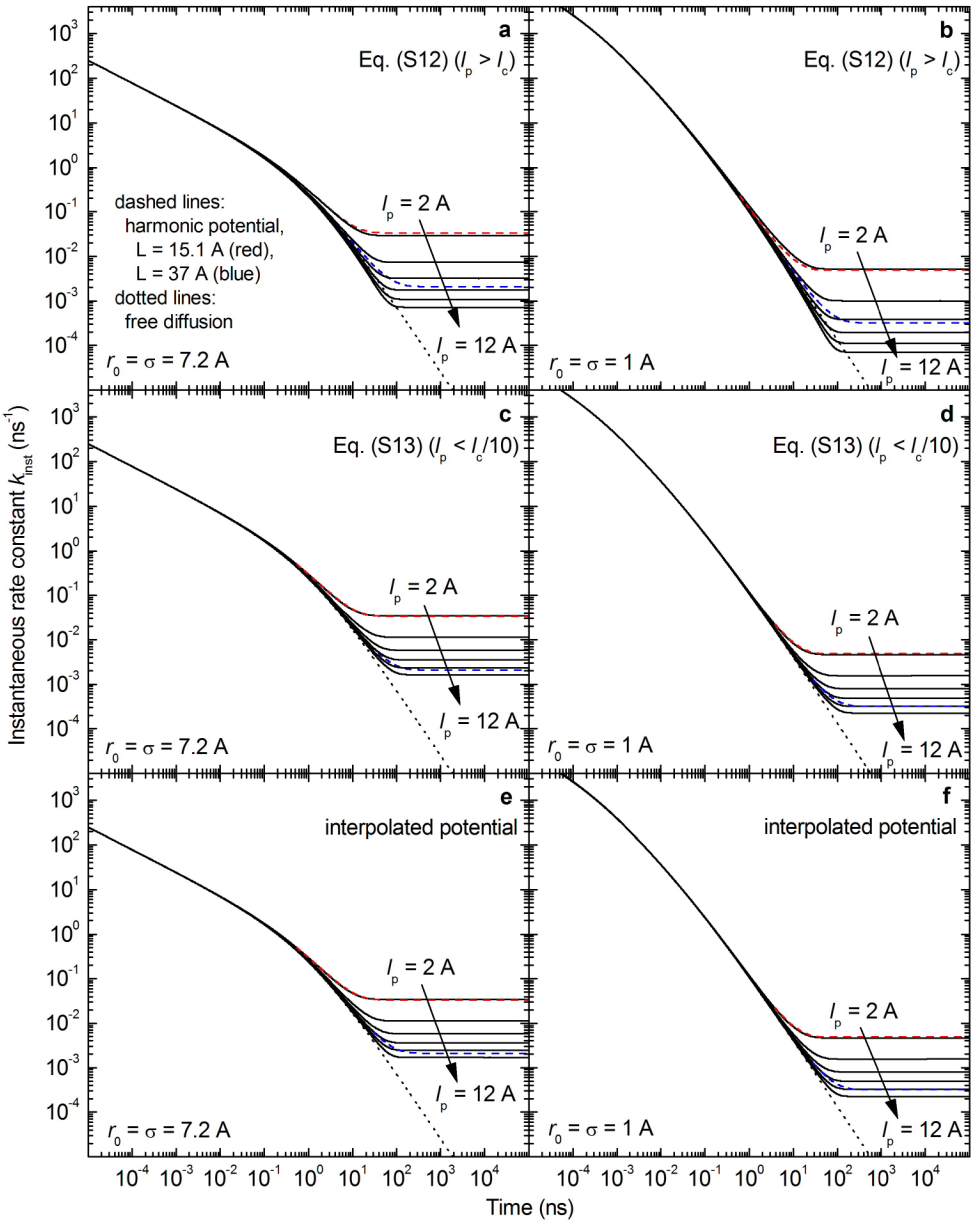

Figure S8. The effect of chain stiffness on the time dependent instantaneous rate constant of geminate recombination, $k_{inst}(t)$, of two radicals which are tethered at the end of a polypeptide chain with N = 15 residues (contour length l_c = 57 Å). $k_{inst}(t)$ was calculated from the survival probability, $P(t)$, obtained numerically assuming diffusion in modified potentials, as described in the text (black solid lines). **a**, **b**: using potential for large bending rigidity ($l_p > l_c$), Eqs. (S11) and (S12); **c**, **d**: using potential for very small bending rigidity ($l_p < l_c/10$), Eq. (S 11) and (S13); **e**, **f**: using the interpolated potential as described in the text. The persistence length, l_p, was varied from 2 Å to 12 Å, as indicated in the figures. Shown are the results for a radical pair with encounter distance σ, initial pair separation r_0 and relative diffusion coefficient D recombining on encounter with a recombination rate coefficient k_{rec} with the following values: D = 4 Å^2/ns; k_{rec} = 1.1 10^{12} cm^{3}mol^{-1}s^{-1}; $r_0 = \sigma$= 7.2 Å (**a** ,**c**, **e**) or $r_0 = \sigma$= 1 Å (**b** ,**d**, **f**). Also shown are the results for diffusion in a harmonic potential, Eq. (S4), with L = 15.1 Å (=$(2l_pl_c)^{1/2}$ for l_p = 2 Å, red dashed lines) and 37 Å (=$(2l_pl_c)^{1/2}$for l_p = 12 Å, blue dashed lines), and the results for free diffusion, calculated from Eq. (S3) (black dotted lines).

times when conformational equilibrium is reached; there is a pronounced effect of l_p on the equilibrium value of $k_{inst}(t)$, similar to that of L in simulations using the harmonic spring model (Fig. S8). There are slight differences between the time dependence of $k_{inst}(t)$ during the transition to equilibrium when taking into account chain stiffness; as expected, this is particularly pronounced when using Eq. (S12), i.e. for polymers with large bending rigidity (Figs. S8 a,b). However, for all cases, these differences are minor and the overall behavior of $k_{inst}(t)$ is very similar. Thus, it can be concluded that chain stiffness effects alone are not expected to drastically alter the radical recombination dynamics and are not able to account for the experimentally observed power law $k_{inst}(t) \sim t^{-0.94}$ over 9 order of magnitude in time. [‡‡]

2.2.2. Excluded Volume Effects

Excluded volume effects also contribute to chain stiffness, but are expected to have additional effects on the end-to-end distance distribution since residues which are distant to each other in the primary sequence cannot occupy the same volume. Buscaglia *et al* (7) reported an analytical expression for the end-to-end distance distribution of a peptide with $N = 11$ residues which takes into account this effect, based on extensive numerical simulations of wormlike chains which discard all conformations where two non-neighboring residues are closer to each other than a hard-sphere diameter d_α:

$$p_{ev}(r) = \frac{t}{\sigma_{ev}^{\,l+1}\Gamma[(l+1)/t]} r^l e^{-(r/\sigma_{ev})^t} \qquad \text{(S14)}$$

Here, l, t and σ_{ev} are numerical parameters which are tabulated in ref. (7) for values of d_α ranging from 0 to 6 Å and $\Gamma(\,)$ is the gamma function.

Figure S9 shows simulations of the instantaneous recombination rate constant based on the effective potential $U_{ev}(r)$, calculated from this end-to-end distribution using Eq. (S11), in the absence ($d_\alpha = 0$) and presence of excluded volume effects, as well as simulations using the harmonic spring potential for comparison.[§§] As with chain stiffness effects, the inclusion of excluded volume effects does not affect the results at short times, but changes the exact time dependence at longer times and affects the equilibrium value of k_{inst}. It has to be noted that the root-mean-square distance increases only slightly (from 18.8 to 23.6 Å) when increasing d_α from 0 to 6 Å, whereas the equilibrium value of $k_{inst}(t)$ decreases significantly, due to the lower probability of forming conformations with small end-to-end distances resulting from excluded volume effects. Taking into account excluded volume affects the time dependence of $k_{inst}(t)$ during the transition to equilibrium; in particular, the transition occurs over a shorter time than for the harmonic potential. However, apart from the easily understood reduced equilibrium values, these effects are only minor and the overall behavior of $k_{inst}(t)$ is very similar to the harmonic spring model. Thus, it can be concluded that even when including excluded volume effects the time dependence of the radical recombination dynamics is not drastically altered and thus also excluded volume effects are not able to account for the experimentally observed uniform power law decay $k_{inst}(t) \sim t^{-0.94}$ over 9 orders of magnitude in time.

2.2.3. Simulations Based on an Empirical End-to-End Distance Distribution

It has been reported that the end-to-end distance distribution taking into account excluded volume effects, $p_{ev}(r)$, given in Eq. (S14) is in some disagreement with experimental FRET

[‡‡] By comparison of the Gaussian distribution $4\pi r^2 \exp(-3r^2/2L^2)$ of the freely jointed chain with the stiff chain distribution $p_{cs}(r)$ given in Eq. (S13), it can be seen that the wormlike chain model yields an equilibrium distribution with a root mean square end-to-end distance $L \approx (2l_p l_c)^{1/2}$, particularly for $l_c >> l_p$. Fig. S8 shows that for $l_c > l_p$ the equilibrium values of k_{inst} obtained with the wormlike chain and harmonic spring models indeed are similar when taking into account this approximation.

[§§] Simulations for $r_0 = \sigma = 1$ Å yield similar results, but are not shown here because of the conceptual inconsistency of assuming a reaction between residues with a hard-sphere diameter of larger than 1 Å occurring at an encounter distance of 1 Å.

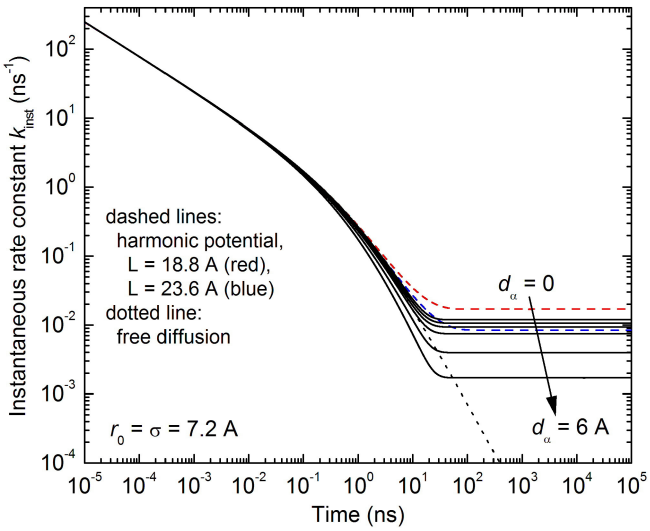

Figure S9. The effect of excluded volume on the time dependent instantaneous rate constant of geminate recombination, $k_{inst}(t)$, of two radicals which are tethered at the end of a polypeptide chain with N = 11 residues (contour length l_c = 42 Å). $k_{inst}(t)$ was calculated from the survival probability, $P(t)$, obtained numerically assuming diffusion in the modified potential calculated from Eqs. (S11) and (S14), as described in the text (black solid lines). The hard-sphere diameter, d_α, was varied from 0 to 6 Å, as indicated in the figure. Shown are the results for a radical pair with encounter distance σ, initial pair separation r_0 and relative diffusion coefficient D recombining on encounter with a recombination rate coefficient k_{rec} with the following values: D = 4 Å^2/ns; k_{rec} = 1.1 10^{12} cm^{3}mol^{-1}s^{-1}; $r_0 = \sigma$ = 7.2 Å. Also shown are the results for diffusion in a harmonic potential, Eq. (S4), with L = 18.8 Å (red dashed line) and 23.6 Å (blue dashed line), corresponding to the root-mean-square distance for d_α of 0 and 6 Å, respectively, and the results for free diffusion, calculated from Eq. (S3) (black dotted line).

results. An empirical skewed Gaussian distribution was suggested instead, which is in better agreement with all empirical results (13):

$$p_{\text{empirical}}(r) = C_{\text{norm}} r^2 e^{-\left(\frac{r-B}{A}\right)^2} \tag{S15}$$

Here, C_{norm} is a normalization constant, whereas A and B are empirical parameters determined from fitting the experimental results. For the peptides (with N = 14 residues) and solvent conditions investigated in ref. (13), A is almost constant at a value of 10-11 Å, and B varies over the range 11-18 Å.

Figure S10 shows simulations of the instantaneous recombination rate constant based on the effective potential $U_{empirical}(r)$, for a range of values of B, corresponding to increasing chain swelling, which is larger than those observed.[***] The results are very similar as those shown in the previous section, Figures S8 and S9, thus showing that the exact details of the end-to-end distance distribution resulting from chain stiffness and excluded volume effects do not significantly affect the radical geminate recombination dynamics and the time dependence of $k_{inst}(t)$.

Therefore, it can be concluded that chain stiffness and excluded volume effects cannot account for the experimentally observed uniform power law decay $k_{inst}(t) \sim t^{-0.94}$ over 9 orders of magnitude in time.

[***] Again, simulations for $r_0 = \sigma$ = 1 Å yield similar results, but are not shown here because of the conceptual problem that Eq. (S15) effectively accounts for excluded volume effects with hard-sphere diameters larger than such short encounter distances.

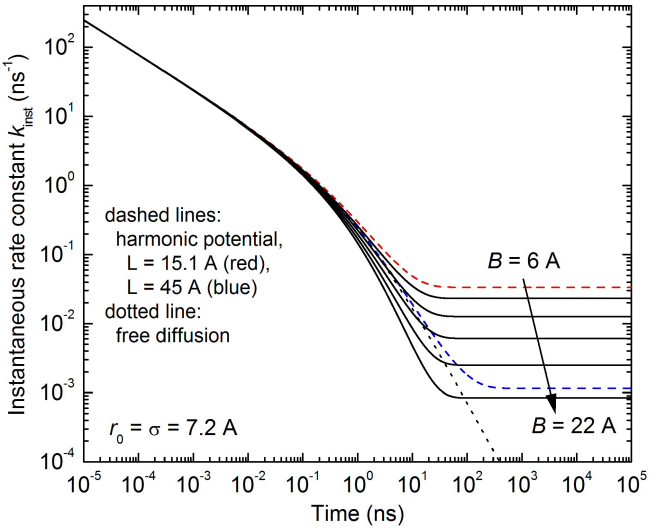

Figure S10. The effect of chain stiffness and excluded volume on the time dependent instantaneous rate constant of geminate recombination, $k_{inst}(t)$, of two radicals which are tethered at the end of a polypeptide chain with N = 14 residues (contour length l_c = 53 Å). $k_{inst}(t)$ was calculated from the survival probability, $P(t)$, obtained numerically assuming diffusion in the modified potential calculated from Eqs. (S11) and (S15), as described in the text (black solid lines). The empirical parameter A was chosen as 11 Å, whereas B was varied from 6 to 22 Å, as indicated in the figure. Shown are the results for a radical pair with encounter distance σ, initial pair separation r_0 and relative diffusion coefficient D recombining on encounter with a recombination rate coefficient k_{rec} with the following values: D = 4 Å^2/ns; k_{rec} = 1.1 10^{12} cm^{3}mol^{-1}s^{-1}; $r_0 = \sigma$ = 7.2 Å. Also shown are the results for diffusion in a harmonic potential, Eq. (S4), with L = 15.1 Å (red dashed line) and 45 Å (blue dashed line), and the results for free diffusion, calculated from Eq. (S3) (black dotted line).

3. Geminate Recombination Governed by Anomalous Diffusion

Anomalous diffusion, where the mean square displacement is nonlinear in time, $\langle r^2(t)\rangle \propto t^{\alpha}$, has been observed widely for the diffusion of biomolecules in the crowded cell environment or in membranes (54, 55); of particular importance is subdiffusional behavior, where $\alpha < 1$. Such subdiffusional behavior can be theoretically rationalized by a wide distribution of trapping times, which in the case of intraprotein subdiffusion have been ascribed to the different barrier heights of the "rugged" potential energy landscape of protein conformation (56, 57). Thus, the motion of the polypeptide backbone, and hence of the thiyl radicals created by UV-photolysis in our experiments, may not be governed by the normal diffusion law, but rather by anomalous diffusion. In the following, we attempt to investigate the effect of subdiffusion on the time-dependence of the survival probability during geminate recombination of these radicals.

3.1. Geminate Recombination of Free Radicals Undergoing Subdiffusive Motion

Diffusional motion in the presence of traps with a wide distribution of trapping times can be theoretically described by the fractional diffusion equation (here given for 1-dimensional diffusion in the force-free case, the extension to 3 dimensions is achieved by replacing $\partial/\partial x$ by the ∇ operator), which has been derived using a continuous time random walk model (58, 59) and can be shown to yield subnormal diffusion, i.e. $\langle r^2(t)\rangle \propto D_\alpha t^{\alpha}$:

$$\frac{\partial}{\partial t} p(x,t) = {}_0D_t^{1-\alpha} D_\alpha \frac{\partial^2}{\partial x^2} p(x,t) \qquad \text{(S16)}$$

where $p(x,t)$ is the probability density of finding a particle at position x at time t, D_α is a generalized diffusion coefficient with dimension $[D_\alpha] = \text{Å}^2\,\text{ns}^{-\alpha}$, and the Riemann-Liouville operator is defined by

$$ {}_0D_t^{1-\alpha} f(x,t) = \frac{1}{\Gamma(\alpha)} \frac{\partial}{\partial t} \int_0^t dt' \frac{f(x,t')}{(t-t')^{1-\alpha}} \tag{S17} $$

However, the use of this fractional diffusion equation, either for explicitly deriving expressions for the re-encounter probability of two radicals at contact distance σ after being created at $t = 0$ at a distance r_0, or for numerical simulations of their survival probability comparable to those described above for normal diffusion, are beyond the scope of this paper.

Instead, we make use of the expression derived by Seki *et al.* for the survival probability, $P(t)$, of a pair of particles undergoing subdiffusive motion and subject to geminate recombination (60). Here, subdiffusive motion is simulated using a continuous time random walk model with a fixed jump size, b, and a waiting time distribution $\psi(t)$ which results from the assumption of an activated jump rate, $\gamma(E)$, with an exponential distribution, $g(E)$, of the activation energy, E:[†††]

$$ \begin{aligned} \gamma(E) &= \gamma_\mathrm{r} e^{-\frac{E}{k_\mathrm{B}T}} \\ g(E) &= \frac{1}{k_\mathrm{B}T_\mathrm{c}} e^{-\frac{E}{k_\mathrm{B}T_\mathrm{c}}} \end{aligned} \tag{S18} $$

where k_B is the Boltzmann constant, T the temperature, $k_\mathrm{B}T_\mathrm{c}$ characterizes the width of the distribution of the jump activation energy and γ_r the maximum (non-activated) jump rate. This model leads to subdiffusive behavior, i.e. the mean square displacement is nonlinear in time: $\langle r^2(t)\rangle \propto t^\alpha$,with $\alpha = T/T_\mathrm{c}$. Geminate recombination was assumed to occur with a first-order rate constant γ_rc when the particles are at the contact distance.

Unfortunately, only the Laplace transform of $P(t)$, $\hat{P}(s)$, can be written in closed form:[‡‡‡]

$$ \hat{P}(s) = \frac{1}{s}\left(1 - \frac{\sigma}{r_0} \frac{e^{-\frac{r_0-\sigma}{\sqrt{\hat{Q}(s)D_\alpha}}}}{1 + \frac{4\pi\sigma D_\alpha}{\hat{k}_\alpha(s)}\left(1 + \frac{\sigma}{\sqrt{\hat{Q}(s)D_\alpha}}\right)}\right) \tag{S19} $$

with

$$ \begin{aligned} \hat{Q}(s) &= \frac{1}{(1-\bar{\psi}(s))\gamma_\mathrm{r}^\alpha} \\ \hat{k}_\alpha(s) &= \left(\bar{\psi}(s) - \bar{\psi}(s+\gamma_\mathrm{rc})\right)\gamma_\mathrm{r}^\alpha 2\pi\sigma^2 b \\ \bar{\psi}(s) &= 1 - \alpha\int_0^1 dy \frac{y^{\alpha-1}}{1+\gamma_\mathrm{r} y/s} \\ D_\alpha &= \frac{1}{2}\gamma_\mathrm{r}^\alpha b^2 \end{aligned} $$

[†††] It has to be noted that this model is a simplified version of the continuous time random walk model used to derive the fractional diffusion equation (28).

[‡‡‡] Factors $(\sin\pi\alpha)/\pi\alpha$ in the expressions for D_α, $\hat{Q}(s)$ and $\hat{k}_\alpha(s)$ which cancel in the final expression for $\hat{P}(s)$ have been omitted here for clarity.

Here, we used the numeric inverse Laplace transformation algorithm developed by Zakian (61) for calculating $P(t)$ from $\widehat{P}(s)$. A value of b of 0.0001 Å was used throughout. In a first step, the model parameters γ_r and γ_{rc} were chosen so that for $\alpha = 1$ the results for $P(t)$ – and consequently for the instantaneous rate constant $k_{inst}(t) = -(dP(t)/dt)/P(t)$ – from Eq. (S3) were reproduced as closely as possible, see Figure S11. It can be seen that the results from Eq. (S3) indeed are well reproduced in all cases.[§§§] The effect of subdiffusion was then studied by decreasing α, keeping all other parameters fixed. For testing the general validity of the conclusions summarized below, simulations were performed for more model parameters than shown here; in all cases, the same general behavior was observed.

Figures S11a,d,g,j show that the time scale over which geminate recombination occurs is significantly stretched by subdiffusional behavior; recombination is expected to last over many orders of magnitude in time for small values of α. This is a first indication that the experimental results reported here, which show geminate recombination to occur over 9 orders of magnitude in time, may be related to subdiffusional behavior of the polypeptide backbone.

An even more intriguing observation can be made when analyzing $k_{inst}(t)$ (Figs. S11b,e,h,k). For $\alpha = 1$, the simulations shown here yield essentially the same result as already obtained from Eq. (S3), namely an initial power law $t^{-0.5}$ which turns into (approximately) $t^{-1.5}$ once diffusion has occurred over the length scale of σ. Most interestingly, upon decreasing α, i.e. increasingly subdiffusional behavior, the power for the initial decrease of $k_{inst}(t)$ *in*creases, whereas that for longer times *de*creases. This is shown more clearly in Figures S11c,f,i,l, which directly show the powers at short and long times obtained from fits of $k_{inst}(t)$. For all sets of parameters, at $\alpha \leq 0.3$, the two "branches" of $k_{inst}(t)$ merge into a single power law, $k_{inst}(t) \propto t^{-n}$, with a power n of the order of 0.95 at $\alpha = 0.3$, which is highly reminiscent of the experimentally observed power law $k_{inst}(t) \propto t^{-0.94}$. Upon further decreasing α, $k_{inst}(t)$ retains essentially single-power law behavior, although the power decreases slightly from the value at $\alpha = 0.3$. Thus, we conclude that our experimental observation, which is not compatible with normal diffusion, is fully compatible with subdiffusional behavior governed by $\langle r^2(t) \rangle \propto t^{\alpha}$ with $a \sim 0.3$.

3.2. Recombination of Tethered Radicals Undergoing Subdiffusive Motion

The simulations for subdiffusive motion described in the previous section do not account for the tethering effect of the polypeptide backbone linking the two radicals. As in the case of normal diffusion, it is expected that the radicals eventually reach an equilibrium distribution, having spread over the full range of possible separation distances, which is limited by the finite length of the linking polypeptide backbone. Once this equilibrium distribution has been reached, the probability density of radical encounter, and hence the instantaneous rate constant for recombination, should not change any further in time, see Figures S4-S10.

In the experiments, no leveling off of $k_{inst}(t)$ was found (Fig. 3), indicating that for N-PGK it takes more than 1 ms to reach polypeptide conformational equilibrium, even in the presence of 8 M urea, when the protein is denatured. This is at least 3 orders of magnitude longer than predicted by simulations assuming normal diffusion of the polypeptide backbone with typical intra-peptide diffusion constants determined from quenching experiments on model peptides, which show a leveling off of $k_{inst}(t)$ on the time scale of 0.1-1 μs (Fig. S5).

The tethering effect of the polypeptide backbone can be accounted for by assuming that the radicals move under the influence of a harmonic potential, see section 1.2 and Eq. (S4). Subdiffusive motion in such a potential can be described by the fractional Fokker-Planck equation for the probability density $p(x,t)$ of finding a particle at position x at time t (62), which in effect is a combination of the Smoluchowski equation of normal diffusion in a harmonic potential, Eq. (S5), and the fractional diffusion equation describing anomalous diffusion, Eq.(S16) (here again written for the 1-dimensional case):

[§§§] It is not clear whether the remaining slight deviations result from limitations of the model, an imperfect choice of the model parameters or the limiations of the numerical inverse Laplace transformation.

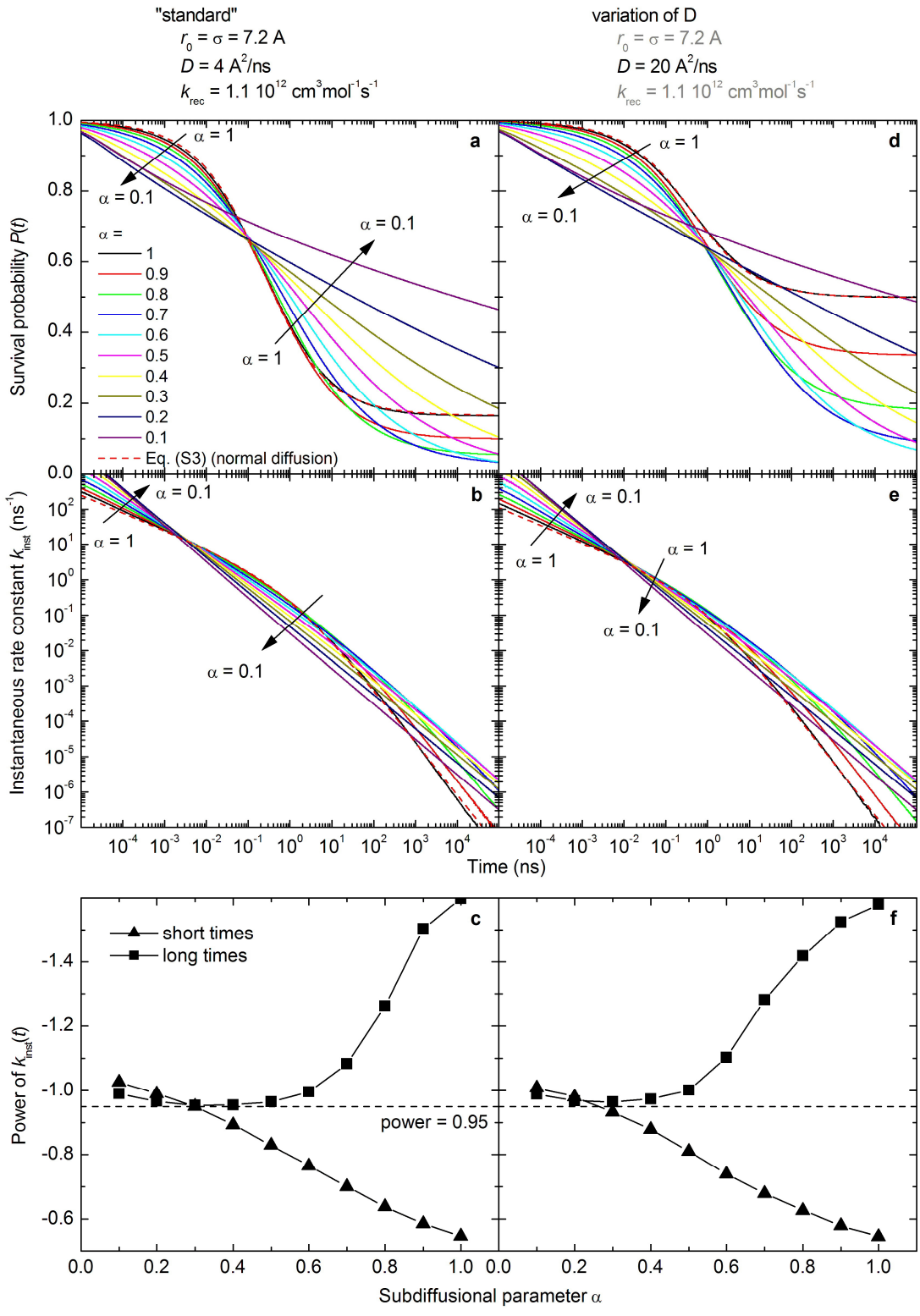

Figure S11. Simulations of geminate recombination of a radical pair created at an initial pair separation r_0, and recombining at the encounter distance σ with a recombination rate coefficient k_{rec}, assuming subdiffusive relative motion of the radicals with a subdiffusive parameter, α, between 0.1 and 1. The relative diffusion coefficient D refers to the case $\alpha = 1$, the choice of parameters for $\alpha < 1$ is described in the text. Shown are the survival probability $P(t)$ (**a**,**d**,**g**,**j**),

…continued on next page

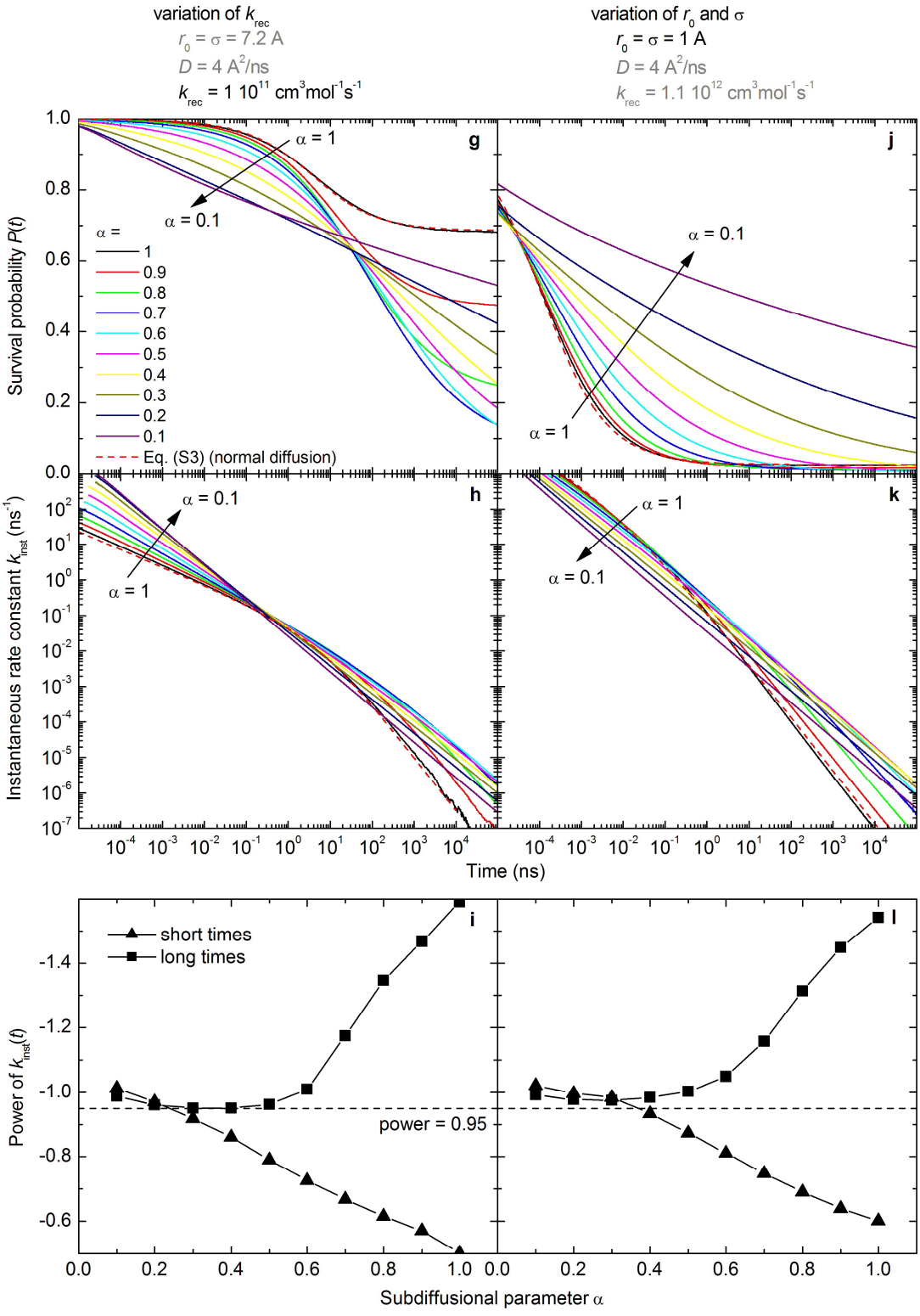

Figure S11 (cont.).
calculated from Eq. (S19), the instantaneous rate constant $k_{inst}(t) = -(dP(t)/dt)/P(t)$ (**b**,**e**,**h**,**k**), and the power of the time dependence of $k_{inst}(t)$ at short and long times, obtained from fits of $k_{inst}(t)$ (**c**,**f**,**i**,**l**). The red dashed lines are the results for normal diffusion ($\alpha = 1$), calculated analytically from Eq. (S3).

$$\frac{\partial}{\partial t} p(x,t) = {}_0D_t^{1-\alpha} D_\alpha \frac{\partial}{\partial x}\left(\frac{\partial}{\partial x} p(x,t) + p(x,t) \frac{\partial}{\partial x} U(x)/kT \right) \quad \text{(S20)}$$

with the Riemann-Liouville operator ${}_0D_t^{1-\alpha}$ as defined in Eq. (S17).

The solution of this equation for long times yields the expected Gaussian equilibrium distribution for a random coil polymer. However, the approach to equilibrium is significantly slower than in the case of normal diffusion. This is exemplified in Figure 20 of reference (59), which describes the spreading of particles within a harmonic potential. In the case of normal diffusion, the transition from the free diffusion behavior at short times to the equilibrium distribution occurs within one magnitude of time, see also Figure S5 above. For subdiffusive motion, this transition is much slower, taking 4 orders of magnitude of time for $\alpha = 0.5$ (Fig. 20 of reference (59)). This is expected to contribute to the fact that no leveling off of $k_{inst}(t)$ is observed in our experimental data even at the longest time scale (1 ms).

In summary, we conclude that our experimental observation, i.e. a uniform power law decay of the instantaneous rate constant for geminate recombination of thiyl radicals bound to a polypeptide or protein backbone, $k_{inst}(t) \sim t^{-0.94}$, over 9 order of magnitude in time, is not compatible with normal diffusional behavior of the polypeptide backbone. On the other hand, intraprotein subdiffusion, modeled by a continuous time random walk with a wide waiting time distribution, predicts the observed behavior perfectly well.

References

1. Milanesi L et al. (2008) A method for the reversible trapping of proteins in non-native conformations. *Biochemistry* 47**:** 13620-13634.
2. Parker MJ, Spencer J, Clarke AR (1995) An integrated kinetic analysis of intermediates and transition states in protein folding reactions. *J Mol Biol* 253**:** 771-786.
3. Lapidus LJ, Eaton WA, Hofrichter J (2000) Measuring the rate of intramolecular contact formation in polypeptides. *Proc Natl Acad Sci USA* 97**:** 7220-7225.
4. Lapidus LJ, Steinbach PJ, Eaton WA, Szabo A, Hofrichter J (2002) Effects of chain stiffness on the dynamics of loop formation in polypeptides. Appendix: Testing a 1-dimensional diffusion model for peptide dynamics. *J Phys Chem B* 106**:** 11628-11640.
5. Krieger F, Fierz B, Bieri O, Drewello M, Kiefhaber T (2003) Dynamics of unfolded polypeptide chains as model for the earliest steps in protein folding. *J Mol Biol* 332**:** 265-274.
6. Möglich A, Krieger F, Kiefhaber T (2005) Molecular basis for the effect of urea and guanidinium chloride on the dynamics of unfolded polypeptide chains. *J Mol Biol* 345**:** 153-162.
7. Buscaglia M, Lapidus LJ, Eaton WA, Hofrichter J (2006) Effects of denaturants on the dynamics of loop formation in polypeptides. *Biophys J* 91**:** 276-288.
8. Fierz B, Kiefhaber T (2007) End-to-end vs. interior loop formation kinetics in unfolded polypeptide chains. *J Am Chem Soc* 129**:** 672-679.
9. Singh VR, Kopka M, Chen Y, Wedemeyer WJ, Lapidus LJ (2007) Dynamic similarity of the unfolded states of proteins L and G. *Biochemistry* 46**:** 10046-10054.
10. Fierz B et al. (2007) Loop formation in unfolded polypeptide chains on the picoseconds to microseconds time scale. *Proc Natl Acad Sci USA* 104**:** 2163-2168.

11. Fierz B, Reiner A, Kiefhaber T (2009) Local conformational dynamics in α-helices measured by fast triplet transfer. *Proc Natl Acad Sci USA* 106**:** 1057-1062.
12. Chen YJ, Parrini C, Taddei N, Lapidus LJ (2009) Conformational properties of unfolded HypF-N. *J Phys Chem B* 113**:** 16209-16213.
13. Soranno A, Longhi R, Bellini T, Buscaglia M (2009) Kinetics of contact formation and end-to-end distance distributions of swollen disordered peptides. *Biophys J* 96**:** 1515-1528.
14. Reiner A, Henklein P, Kiefhaber T (2010) An unlocking/relocking barrier in conformational fluctuations of villin headpiece subdomain. *Proceedings of the National Academy of Sciences of the United States of America* 107**:** 4955-4960.
15. Voelz VA, Singh VR, Wedemeyer WJ, Lapidus LJ, Pande VS (2010) Unfolded-state dynamics and structure of protein L characterized by simulation and experiment. *J Am Chem Soc* 132**:** 4702-4709.
16. Hudgins RR, Huang F, Gramlich G, Nau WM (2002) A fluorescence-based method for direct measurement of submicrosecond intramolecular contact formation in biopolymers: An exploratory study with polypeptides. *J Am Chem Soc* 124**:** 556-564.
17. Neuweiler H, Schulz A, Bohmer M, Enderlein J, Sauer M (2003) Measurement of submicrosecond intramolecular contact formation in peptides at the single-molecule level. *J Am Chem Soc* 125**:** 5324-5330.
18. Nettels D, Hoffmann A, Schuler B (2008) Unfolded protein and peptide dynamics investigated with single-molecule FRET and correlation spectroscopy from picoseconds to seconds. *J Phys Chem B* 112**:** 6137-6146.
19. Hagen SJ, Hofrichter J, Szabo A, Eation WA (1996) Diffusion-limited contact formation in unfolded cytochrome c: Estimating the maximum rate of protein folding. *Proc Natl Acad Sci USA* 93**:** 11615-11617.
20. Hagen SJ, Carswell CW, Sjolander EM (2001) Rate of intrachain contact formation in an unfolded protein: Temperature and denaturant effects. *J Mol Biol* 305**:** 1161-1171.
21. Scott TW, Liu SN (1989) Picosecond geminate recombination of phenylthiyl free-radical pairs. *J Phys Chem* 93**:** 1393-1396.
22. Bultmann T, Ernsting NP (1996) Competition between geminate recombination and solvation of polar radicals following ultrafast photodissociation of bis(p-aminophenyl) disulfide. *J Phys Chem* 100**:** 19417-19424.
23. Hagen SJ, Hofrichter J, Eaton WA (1997) Rate of intrachain diffusion of unfolded cytochrome *c*. *J Phys Chem B* 101**:** 2352-2365.
24. Möglich A, Joder K, Kiefhaber T (2006) End-to-end distance distributions and intrachain diffusion constants in unfolded polypeptide chains indicate intramolecular hydrogen bond formation. *Proc Natl Acad Sci USA* 103**:** 12394-12399.
25. Jones CM et al. (1993) Fast events in protein folding initiated by nanosecond laser photolysis. *Proc Natl Acad Sci USA* 90**:** 11860-11864.
26. Nettels D, Gopich IV, Hoffmann A, Schuler B (2007) Ultrafast dynamics of protein collapse from single-molecule photon statistics. *Proc Natl Acad Sci USA* 104**:** 2655-2660.
27. Shin KJ, Kapral R (1978) Kinetic theory of reactive pair dynamics in liquids. *J Chem Phys* 69**:** 3685-3696.
28. Morine GH, Kuntz RR (1979) Spectral shifts of the p-aminophenylthiyl radical absorption and emission in solution. *Chem Phys Lett* 67**:** 552-554.

29. Milanesi L, Reid GD, Beddard GS, Hunter CA, Waltho JP (2004) Synthesis and photochemistry of a new class of photocleavable protein cross-linking reagents. *Chem Eur J*: 1705-1710.
30. Borisevich NA, Lysak NA, Melnichuk SV, Tikhomirov SA, Tolstorozhev GB (1990) in *Ultrafast Phenomena in Spectroscopy*, eds. Klose, E. & Wilhelmi, B. (Springer, Berlin, Heidelberg), Vol. 49, pp. 276-281.
31. Volk M et al. (1997) Peptide conformational dynamics and vibrational Stark effects following photoinitiated disulfide cleavage. *J Phys Chem B* 101: 8607-8616.
32. Borisevich NA, Buganov OV, Dubovskii VL, Tikhomirov SA, Tolstorozhev GB (2005) Femtosecond dynamics of geminate recombination of radicals upon photodissociation of aromatic disulfides. *Opt Spectrosc* 98: 368-373.
33. Wilemski G, Fixman M (1974) Diffusion-controlled intrachain reactions of polymers. I. Theory. *J Chem Phys* 60: 866-877.
34. Wilemski G, Fixman M (1974) Diffusion-controlled intrachain reactions of polymers. II. Results for a pair of terminal reactive groups. *J Chem Phys* 60: 878-890.
35. Doi M (1975) Diffusion-controlled reaction of polymers. *Chem Phys* 9: 455-466.
36. Sunagawa S, Doi M (1975) Theory of diffusion-controlled intrachain reactions of polymers. *Polymer J* 7: 604-612.
37. Szabo A, Schulten K, Schulten Z (1980) First passage time approach to diffusion controlled reactions. *J Chem Phys* 72: 4350-4357.
38. de Gennes PG (1982) Kinetics of diffusion-controlled processes in dense polymer systems. I. Nonentangled regimes. *J Chem Phys* 76: 3316-3321.
39. Yeung C, Friedman B (2005) Cyclization of Rouse chains at long- and short-time scales. *J Chem Phys* 122: 214909.
40. Brant DA, Flory PJ (1965) The configuration of random polypeptide chains. *J Am Chem Soc* 87: 2788-2791.
41. Miller WG, Brant DA, Flory PJ (1967) Random coil configurations of polypeptide copolymers. *J Mol Biol* 23: 67-80.
42. Schwarz G (1968) Kinetic analysis by chemical relaxation methods. *Rev Mod Phys* 40: 206-218.
43. Thompson PA, Eaton WA, Hofrichter J (1997) Laser temperature jump study of the helix⇔coil kinetics of an alanine peptide interpreted with a 'kinetic zipper' model. *Biochemistry* 36: 9200-9210.
44. Rouse PR (1953) A theory of the linear viscoelastic properties of dilute solutions of coiling polymers. *J Chem Phys* 21: 1272-1280.
45. Zimm BH (1956) Dynamics of polymer molecules in dilute solution: Viscoelasticity, flow birefringence and dielectric loss. *J Chem Phys* 24: 269-278.
46. Yamakawa H, Stockmayer WH (1972) Statistical mechanics of wormlike chains. 2. Excluded volume effects. *J Chem Phys* 57: 2843-2854.
47. Wilhelm J, Frey E (1996) Radial distribution function of semiflexible polymers. *Phys Rev Lett* 77: 2581-2584.
48. Kratky O, Porod G (1949) Röntgenuntersuchung gelöster Fadenmoleküle. *Recl Trav Chim* 68: 1106-1122.
49. Klimov DK, Thirumalai D (2002) Stiffness of the distal loop restricts the structural heterogeneity of the transition state ensemble in SH3 domains. *J Mol Biol* 317: 721-737.

50. Zhou HX (2001) Loops in proteins can be modeled as worm-like chains. *J Phys Chem B* 105**:** 6763-6766.
51. Kellermayer MSZ, Smith SB, Ganzier HL, Bustamante C (1997) Folding-unfolding transitions in single titin molecules characterized with laser tweezers. *Science* 276**:** 1112-1116.
52. Rief M, Gautel M, Schemmel A, Gaub HE (1998) The mechanical stability of immunoglobulin and fibronectin III domains in the muscle protein titin measured by atomic force microscopy. *Biophys J* 75**:** 3008-3014.
53. Wang K, Forbes JG, Jin AJ (2001) Single molecule measurements of titin elasticity. *Prog Biophys Molec Biol* 77**:** 1-44.
54. Dix JA, Verkman AS (2008) Crowding effects on diffusion in solutions and cells. *Annu Rev Biophys* 37**:** 247-263.
55. Horton MR, Höfling F, Rädler JO, Franosch T (2010) Development of anomalous diffusion among crowding proteins. *Soft Matter* 6**:** 2648-2656.
56. Luo G, Andricioaei I, Xie XS, Karplus M (2006) Dynamic distance disorder in proteins is caused by trapping. *J Phys Chem B* 110**:** 9363-9367.
57. Garcia AE, Hummer G (1999) Conformational dynamics of cytochrome c: Correlation to hydrogen exchange. *Proteins* 36**:** 175-191.
58. Barkai E, Metzler R, Klafter J (2000) From continuous time random walks to the fractional Fokker-Planck equation. *Phys Rev E* 61**:** 132-138.
59. Metzler R, Klafter J (2000) The random walk's guide to anomalous diffusion: A fractional dynamics approach. *Phys Rep* 339**:** 1-77.
60. Seki K, Wojcik M, Tachiya M (2003) Recombination kinetics in subdiffusive media. *J Chem Phys* 119**:** 7525-7533.
61. Zakian V (1970) Rational approximation transfer-function matrix of distributed system. *Electron Lett* 6**:** 474-476.
62. Metzler R, Barkai E, Klafter J (1999) Anomalous diffusion and relaxation close to thermal equilibrium: A fractional Fokker-Planck equation approach. *Phys Rev Lett* 82**:** 3563-3567.